Optimal Design and Control of Variable Impedance Actuated Robots

by

Altay Zhakatayev

Submitted in partial fulfillment of the requirements for the degree of PhD in Science, Engineering and Technology

at the

NAZARBAYEV UNIVERSITY

October 2019

2
Optimal Design and Control of Variable Impedance Actuated Robots by

Altay Zhakatayev

Submitted to the Department of Robotics and Mechatronics
on October 15, 2019, in partial fulfillment of the
requirements for the degree of
PhD in Science, Engineering and Technology

Abstract

In this thesis, the challenging problems of design and control of variable impedance actu ated robots are considered. The difficulties arise due to nonlinear dynamics, physical con straints of the system, and presence of additional actuators and nonlinear elastic/damping elements. As a result, we propose a control methodology, which takes into account system constraints and input bounds, guarantees system utilization to its full potential, and closely achieves the system's target performance level. The thesis consists of seven chapters. The first chapter gives a broad introduction to the problem and provides the literature review. For example, differences between position-controlled robots and variable impedance actu ated robots are discussed, their corresponding advantages and disadvantages are presented and compared, past design and control solutions are reviewed, and the hypothesis is de scribed. The second chapter covers the proposed closed-loop control methodology for variable stiffness actuated robots. This chapter covers the general idea behind closed-loop control of variable

impedance actuated robots using model predictive control, and it also includes simulations and experimental results. The augmentation of the variable stiffness robots with reaction wheels is described in chapter three. Specifically, the advantages of using reaction wheels to actuate the variable stiffness robots are discussed. This is fol lowed by a discussion of time-optimal control of variables stiffness robots in chapter four. This chapter presents and describes two time-optimal control problems: minimum time for target performance and minimum time for maximum performance. In chapter five energy optimal control of variable stiffness robots is described. In particular, three energy-optimal control problems are defined: maximum performance with limited energy, target perfor mance with minimum energy and maximum performance with minimum energy. Then chapter six contains successive linearization-based model predictive control of variable stiffness robots. The main idea of this chapter is that linearization might be beneficial for model predictive control of nonlinear systems due to a simpler model and the resulting smaller sampling time. Finally, chapter seven describes the potential impact of our research in the field of robotics and society.

Thesis Supervisor: Huseyin Atakan Varol
Title: Professor and Chair of Robotics

4

Contents

List of Figures

List of Tables

List of publications co-authored by the candidate in relation to the thesis work:

· Zhakatayev, A., Rubagotti, M., Varol, H. A. “Integrated optimal design and control of variable stiffness actuated robots”, European Control Conference (ECC), Linz, Austria, pp.1100-1105, 2015.

· Zhakatayev, A., Baimyshev, A., Varol, H. A. “A preliminary study for using reac tive braking torque in variable impedance actuation”, International Symposium on System Integration (SII), Nagoya, Japan, pp.754-759, 2015.

· Zhakatayev, A., Rubagotti, M., Varol, H. A. “Closed-Loop Control of Variable Stiff ness Actuated Robots via Nonlinear Model Predictive Control”, IEEE

Access, pp. 235-248, Vol. 3, 2015.

· Baimyshev, A., Zhakatayev, A., Varol, H. A. “Augmenting Variable Stiffness Actua tion Using Reaction Wheels”, IEEE Access, pp. 4618-4628, Volume 4, 2016.

· Zhakatayev, A., Rubagotti, M., Varol, H. A. “Time Optimal Control of Variable Stiff ness Actuated Robots”, IEEE/ASME Transactions on Mechatronics, pp. 1247-1258, Volume: 22, Issue: 3, 2017.

· Zhakatayev, A., Rakhim, B., Adiyatov O., Baimyshev, A., Varol, H. A. “Succes sive Linearization Based Model Predictive Control of Variable Stiffness Actuated Robots”, IEEE Advanced Intelligent Mechatronics (AIM), Munich, Germany, pp. 1774-1779, 2017.

· Zhakatayev, A., Rubagotti, M., Varol, H. A. “Energy-Aware Optimal Control of Vari able Stiffness Actuated Robots”, IEEE Robotics and Automation Letters, pp. 330- 337, Vol. 4, Issue 2, 2019.

Abbreviations

· OCP - optimal control problem

· MPC - model predictive control

· NMPC - nonlinear model predictive control ·

FHOCP - finite-horizon optimal control

problem · VIA - variable impedance actuated

· VSA - variable stiffness actuated

· VDA - variable damping actuated

· QP - quadratic programming

· SQP - sequential quadratic

programming · NEE - nonlinear elastic

elements

· SEA - Series Elastic Actuator

· DOF - degree of freedom

· SMA - shape memory alloy

· LQR - linear quadratic regulator

· LMPC - linearized MPC

· RMSE - root mean square error

Acknowledgments

Many people contributed to my PhD, including:

· my advisor Professor Huseyin Atakan Varol from Robotics and Mechatronics De partment, School of Engineering and Digital Sciences, Nazarbayev

University, whom I thank for his mentorship, unswerving advocacy, delightful collegiality, parental guidance and extensive teaching.

· my co-supervisors Associate Prof. Matteo Rubagotti and Associate Prof. Michele Folgheraiter from Robotics and Mechatronics Department, School of Engineering and Digital Sciences, Nazarbayev University, for their guidance and teaching.

· my external supervisor Associate Prof. Frank Sup from Mechanical and Industrial Engineering, University of Massachusetts Amherst.

· my current ARMS lab colleagues Bexultan Rakhim, Denis Fadeyev, Askat Kuzdeuov, Akmaral Moldagalieva.

· my past lab colleagues Olzhas Adiyatov (currently a PhD student at the University of Waterloo, Canada), Almaskhan Baimyshev (currently a PhD student at the Vanderbilt University, USA).

· my colleagues and friends at NU.

· my grandmother Aziza, parents Bakhyt and Toxan, my sister Ainur, and my family Leila, Alimzhan and Rayana.

· finally thanks to the Creator for the guidance and blessings.

Declaration

I declare that the research contained in this thesis, unless otherwise formally

indicated within the text, is the original work of the author. The thesis has not been previously submitted to this or any other university for a degree, and does not incorporate any material already submitted for a degree.

Signed

Dated

Notation

The following notation will be used throughout the thesis. Sets of reals, positive reals, non-negative integers, and positive integers would be denoted as R, $R_{>0}$, $Z_{\geq 0}$, and $Z_{>0}$, respectively. Given a vector $\mathbf{x} \in R^{n}$, $\mathbf{x}'$ denotes its transpose, and $\|\mathbf{x}\|$ denotes its Euclidean norm. Similarly, given a square matrix $\mathbf{A} \in R^{n \times n}$, $\mathbf{A}'$ denotes its transpose. Positive and semi-positive definiteness of a symmetric matrix $\mathbf{A} = \mathbf{A}'$ are indicated as $\mathbf{A} > 0$ and $\mathbf{A} \geq 0$, respectively. Given $\mathbf{x} \in R^{n}$ and $\mathbf{A} \in R^{n \times n}$, the weighted Euclidean norm is defined as $\|\mathbf{x}\|_{\mathbf{A}}$, $(\mathbf{x}'\mathbf{A}\mathbf{x})^{1/2}$. A diagonal matrix $\mathbf{D} \in R^{n \times n}$ with its diagonal elements $d_1, d_2, \ldots, d_n$ is referred to as $\mathbf{D} = \mathrm{diag}(d_1, d_2, \ldots, d_n)$.

Chapter 1

Introduction

1.1 Trends and Future of the Robotics

Robots revolutionized the manufacturing industry. The first industrial robot was installed by General Motors in its factory in New Jersey in 1962 [2]. Since then, the robots changed the industry, and their numbers are growing. According to the International Federation of Robotics Executive Summary, it is estimated that more than 500,000 manufacturing robots will be produced in the 2020 year alone [3], see Fig. 1-1. As the production of robots has increased, their cost has decreased. For example, beginning with the 1990s, the cost of human labor has steadily increased, while in contrast, the price of robots has gradually decreased [4]. Lower production, operation, and maintenance costs associated with the robots make them attractive solutions for manufacturing companies. Additionally, due to the reduced price tag of the robots, small and medium companies are able to employ them in their operation. In other words, the barrier cost for utilization of robots is decreasing by time. Also outsourcing to low-wage countries, the desire of consumers to customization and disruptive technologies make it difficult for manufacturers based on traditional pro duction lines to survive in the modern competitive world [5]. This will enable the further proliferation of small to medium robots, which will be used extensively in in-house produc tions and services. The trend toward automation drives upward the demand for industrial robots. This trend will gradually reshape the labor market and will impact societies. This process has already made a profound impact on post-industrialized towns in the developed

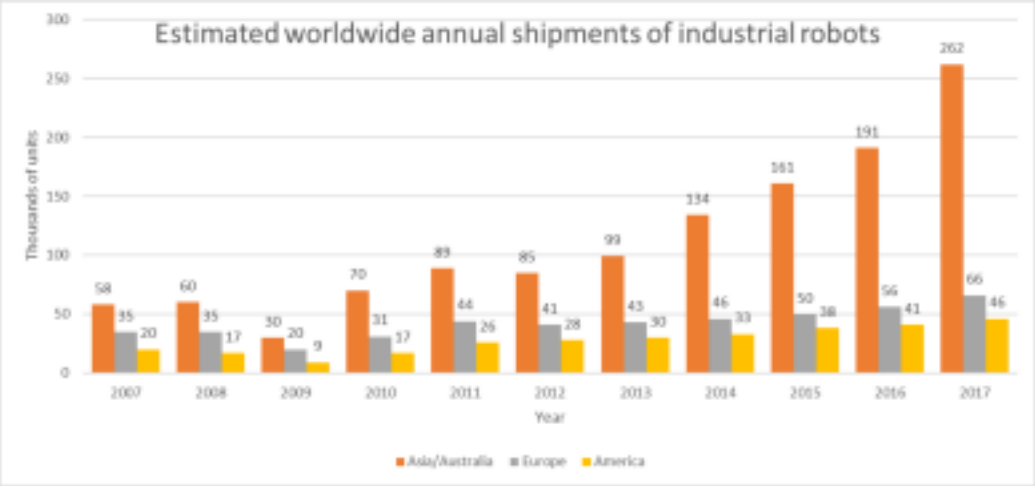

Figure 1-1: Estimated worldwide annual shipments of industrial robots adapted from International Federation of Robotics Executive Summary.

part of the world [6].

The robot utilization is common in the automotive and electrical/electronics industries. They are also used in dangerous and hazardous environments, which pose a significant risk to human workers. Despite the considerable progress in the efficiency and produc tivity of manufacturing achieved with the employment of robots, there are still pressing issues. For example, improving productivity, reducing cost and ecological footprint of the robots, transforming from analog to digital operations, meeting the demand of customers are current hurdles faced by the manufacturing industry [7].

Finding successful solutions to these problems would also assist in achieving the goals of Industry 4.0. In order to understand Industry 4.0, it would be beneficial to review the previous three industrial revolutions. The first industrial revolution involved mechanization using steam and water power. It originated in Britain in the 18th century and then spread to other parts of the world [8]. As a result of the first industrial revolution, agrarian and handicraft based manufacturing were gradually transformed into the industry and machine based manufacturing, while textile and metallurgy was advanced the most. The second industrial revolution involved the development of mass production using assembly lines and electrification [9]. It is estimated to take place at the end of the 19th century and at the beginning of the 20th century. At the end of the second

industrial revolution machine tools, railroads, telegraph and chemical industries flourished [10]. The third industrial revolu

tion involved the computerization and automation of the production process. It is started around the 1950s and is characterized by the emergence of semiconductor technologies, the Internet, and personal computers [11]. Therefore, the third industrial revolution is also called the digital revolution. Each industrial revolution resulted in profound changes in the global society. Urbanization steadily increased, workforce profile changed, new profes sions emerged, while old ones disappeared completely. Now we are located at a specific moment in time, which is the ending of the third industrial revolution and the beginning of the fourth one. Fourth industrial revolution can be described by the advent of the “cyber physical systems”, which provides new capabilities for people and machines [12]. Industry 4.0 is partially based on the technologies and infrastructure of the third industrial revo lution. However, it also involves new groundbreaking technologies such as 3D printing, Internet of Things, virtual and augmented reality, blockchain, machine and artificial intelli gence, smart materials, nanotechnologies, genome editing and so on. The fourth industrial revolution also involves new ways in which technology is embedded in society [12]. Ac cording to experts, smart machines and robots will become smarter as they collect more data. This will make the manufacturing process more efficient and productive, at the same time reducing the waste [9]. Data sharing and communication of different machines and units with each other is what makes the Industry 4.0 revolutionary and powerful. Manufac turers will get the opportunity to modify their production process online in order to meet the demand of customers and markets. One feature of Industry 4.0 is the emergence of the so-called “sharing economy”. Sharing economy describes societal networks, which share certain items or goods. For example, it is estimated that in the future people will share cars, instead of owning them [13]. Industry 4.0 brings new opportunities and, at the same time, threats to our society. Threats include high-income inequality, cyber-security and potential loss of identity [12]. One of the goals of

Industry 4.0 is to enable manufacturers to produce a small series of unique, customized and high-quality products at a competitive price and in a short time. Utilization of robots is viewed as a crucial component to achieving this goal. However, there are yet unresolved issues related to robots, which need to be solved in order to bring Industry 4.0 into reality.

The first problem is a safety of a robot and of a human operator. Nowadays,

when 21

industrial robots are operating in a closed environment, their workspace is constrained by hard walls. This ensures safety from accidental injuries and/or death of a human by pre venting him/her to enter into robot's workspace during its operation. At the same time, the wall prevents damage of a robot due to collisions. Despite the preventive measures, deadly accidents involving industrial robots still happen [14, 15]. However, close physical human-robot interaction is seen as a crucial component of the future manufacturing indus try. Therefore, traditional wall separation of robots can not be maintained for a long time without compromising the industrial needs of mankind in the future. It is envisioned that gradually the robots will perform more tasks related to cooperation with humans. There fore robots need to be made human-friendly, i.e. robots should not pose a threat or danger during interaction with humans. In other words, robots should possess agility and dexterity similar to humans and animals, and should not be very stiff and rigid. It was shown that hu mans and animals modify the impedance of their joints during everyday activities [16, 17]. For example, while performing positioning tasks, like in a pick and place operation, mus cles become stiff. While during tasks involving fast motion, like running and jumping, muscles become loose.

The second problem is energy efficiency. About two-thirds of energy consumption in industry is attributed to the motors [18]. Position controlled robots, which utilize step motors in open-loop control, require a continuous input of energy during their motion and even during stand-still [19]. For example, a robot

consumes energy during both the lifting and lowering of a payload. However, it would be more advantageous if energy is spent only during lifting stage, and if gravity does work during lowering of a payload. This problem might be alleviated by closed-loop current control, which might reduce the power consumption of step motors by as much as 60 % [19]. According to another study, by minimizing the acceleration and deceleration of robots, and by minimizing the time dura tion of their standstill, their energy consumption might be reduced by up to 30 % [20]. In other words, simple trajectory optimization might lead to the increased energy efficiency of robots, while still preserving their performance criteria. Due to the trend that robots are made to perform more human-like tasks, properties such as safety and energy efficiency are prioritized over the accuracy, precision, and repeatability [21]. The importance of this

trend will supposedly grow in the future.

The third problem is the agility and dexterity of robot motion. Robots are taking more jobs traditionally performed by humans, and they exhibit more skills. For example, there are robots which paint a portrait [22], solve Rubik's cube [23], pick and sort objects [24] and much more. However, despite these amazing examples, robots still lack agility and dexterity necessary for operation in an unknown environment or outside of the carefully designed labs. For example, the results of the DARPA Robotics Challenge (DRC) con ducted in 2015 demonstrated that robots still lack the basic skills needed to perform simple tasks, which are commonly performed by humans. The different tasks included opening and passing through a door, driving a car, opening a valve with circular handle, ascending a stair and more [25]. The DRC challenge was devised as a response to Fukushima nuclear disaster and its results outline the directions in which the robots need to be improved.

1.2 Mechanical Impedance

Mechanical dynamics is utilized extensively during the design of most of the structures today. This is attributed to increased light structures, higher speeds, and environmental concerns. Stronger materials and efficient computer-based design tools allow mechanical designs with minimum mass and volume. Additionally, more powerful actuators result in higher rotational and translational speeds of mechanical systems. This, in turn, ne cessitates analysis for structural resonance. Environmental concerns include reduction of acoustic noise and of mechanical vibrations. The field of structural mechanics flourished due to the above factors. When external sinusoidal force is applied to a rigid object, it starts to oscillate back and forth. Mechanical impedance is defined as a complex ratio of external harmonic force to the resultant velocity of an object [26, 27]. In the field of mechanical vibrations, mechanical impedance is defined as a complex ratio of force to dis placement [28]-Sec. 3.5, [29]-Sec. 7.3, [30] Sec. 3.6. It can also be called as resistance for vibration according to an applied vibration. Broadly speaking, mechanical impedance represents amplitude and phase relationship between input (force, torque) and output (trans lational and rotational displacement, velocity). Therefore, it has close similarities with the

transfer function definition from system dynamics. In other words, mechanical impedance is the transfer function of the mechanical system when force is chosen as input and the resulting velocity of an object is output. Given sinusoidal dynamic force $F = F_0 e^{j\omega t}$, with its amplitude F_0 and frequency ω, applied to a rigid body, it results in steady sinusoidal oscillations. Velocity of oscillations is $v = v_0 e^{j(\omega t+\phi)}$, where v_0 and ϕ are, respectively, the amplitude and phase of the velocity. Then mechanical impedance can be defined as

$$Z = \frac{F}{v} = \frac{F_0 e^{j\omega t}}{v_0 e^{j(\omega t+\phi)}} \quad (1.1)$$

Mechanical impedance is a complex quantity. Its real part is called *resistance*, while imag inary component is called *reactance*. Resistance characterizes

dissipation of energy, while reactance describes the transformation of energy from one form to another (storage of en ergy) [31]. There are three mechanical elements: mass, damper, and spring. Mechanical impedance depends on these three parameters. Any mechanical system, no matter how complicated, can be represented as a combination of these three elements. From the defi nition (1.1) it is clear that amplitude of the impedance is linearly decreasing with respect to frequency for spring, is constant for a damper, and is linearly increasing with respect to frequency for a mass. While the phase of the impedance is constant $\frac{\pi}{2}$ for a mass, is zero for a damper and is constant with the value $-\frac{\pi}{2}$ for a spring. Experimental measurement techniques of mechanical impedance were discussed in [32].

1.3 Actuators

There are different types of actuators in existence today. Hydraulic, pneumatic, electric and mechanical actuators are some examples of their different types. Actuators are selected based on the application area and the requirements. In this work, our focus is primarily on electromechanical actuators. Electromechanical actuators can be brushed and brush less. Brushed actuators typically have winding on a rotor and magnets on a stator, while brushless actuators have an opposite arrangement (winding on a stator and magnets on a rotor). Actuators can be geared and ungeared. Ungeared actuators are highly backdrivable,

safe, have high bandwidth and they can be seen as ideal force sources [21]. However, they have limitations in maximum power and forces. This means that ungeared actuators are not suitable for energetic tasks and cannot reject large disturbances. Geared actuators possess qualities from the opposite side of the spectrum. They are non-backdrivable, have accurate positioning, and can generate large forces. This allows them to reject well external dis turbances, and therefore geared actuators can be considered as ideal position sources [21].

However, collision forces generated during impacts of geared actuators are large. As a result, geared actuators are not safe. Both geared and ungeared actuators have no energy storage capabilities and they generate low peak power. In between geared and ungeared ac tuators, there are fixed and variable impedance actuators (VIA). Fixed impedance actuators have constant and finite impedance. In contrast, VIA can modify their mechanical proper ties (impedance), which is the key property and is the source of their advantages relative to geared, ungeared actuators and constant impedance actuators. For fixed and variable impedance actuators, there is a concept of equilibrium. In other words, link of the VIA can deviate from its preset equilibrium position under the influence of external force/torque. If external force/torque is removed, then a link returns to its equilibrium position. For rigid actuators, the concept of equilibrium does not exist [33]. Variable impedance actuators can generate large forces and torques, can store energy and have high peak power. Addi tionally, they have low impact forces, which makes them safe for human-robot interaction (HRI) tasks. Also, the force dynamic range is larger for variable impedance actuators. However, VIA has low bandwidth and suffer in positioning accuracy. In summary, the ad vantages of the variable impedance actuators can be grouped into the following three main categories

1. Safety. This includes low collision forces, low link-side inertia, low friction and dampening of torque/force ripples.

2. Energy storage capability. Due to higher peak torque and velocity characteristics, this includes the ability to perform energetic tasks, such as throwing, jumping, kicking, which require high peak power.

3. Adjustable dynamics. This includes a larger range of task performance,

overcome controller limitations, tunable gait/walking/jumping dynamics.

Fixed impedance actuators are also safe and can store energy, but they can not

adjust their dynamics. Next descriptions of the different ways to achieve VIA are described.

1.4 Variable Impedance Actuators

There are two main methods of how VIA-type performance can be achieved by actua tors [34]. The first is the so-called *active* method, which is based on the utilization of force/torque/velocity sensors to control the robots in the closed-loop. Active methods also employ advanced controllers, which are designed to detect abnormalities during robot op eration (collision, breaking) through data coming from sensors and to react accordingly. These methods can also be called “software”-based method. Active method can transform traditional rigid industrial robots into VIA-type robots. Therefore the active method be stows rigid robots with safety and adjustable dynamics features. DLR’s lightweight robot is an example of a robot with an active compliance [35]. It has features like a high load to own weight ratio, joint torque control, increased flexibility, and fully integrated electronics. However active compliance methods can not empower rigid robots with energy storage ca pabilities. Additionally, these methods are restricted by the limitations of controllers. For example, the sampling time of the controllers puts a limit on the maximum velocity of robot links in order to satisfy certain safety criteria. This is due to the inability of a controller to react accordingly if collision time is much shorter than a sampling time. Therefore there is another, so-called *passive* method, which is “hardware” based design of VIA robots. From a mechanical point of view, VIA is designed and constructed by incorporating nonlinear elastic and damping elements into the actuator, or between an actuator and a link. As a result, a link is mechanically decoupled from an actuator. Therefore inertia as “seen” on the link side is much less than inertia with geared actuators. This is the reason for lower collision forces. Mechanical decoupling of the actuator causes the aforementioned reduc tion in force and velocity bandwidth, and also in less positioning accuracy of the actuators. Passive VIA is the key to enable the robots’ motion to match that of humans and animals. In fact,

by contracting and relaxing the antagonistic muscles, humans can change the stiffness

of the joints [36], which is beneficial at performing various tasks.

We note that due to mechanical decoupling, VIA joints have the output equilibrium position for a link. If external torques and disturbances are applied to a link, then its actual position might be different than its equilibrium position. The equilibrium position is controlled by an actuator, i.e. it can be set by a controller. However, the actual position of the link is not controllable. If the external disturbances and torques are removed, then the link ideally returns to its equilibrium position. For a rigid robot joint, there is no equilibrium position. In other words, for rigid robots, the link is located in a position controlled by an actuator [37]. For VIA joints, actual and desired output positions are different, while for rigid joints, output and desired positions are the same.

Passive variable impedance actuated robots are viewed as a main solution to the afore mentioned three challenges in the robotics [34]. In other words, firstly, VIA joints provide intrinsic safety property for robots [38]. Intrinsic safety property is very important because it does not depend on any external hardware or software. For example, the aforementioned active method to achieve VIA-type performance does not solve the safety problem at the fundamental level. If the controller fails during the operation of the active VIA robot, then it loses its safety property. This means that active VIA robots still pose “hidden” risk. Secondly, passive VIA robots can store energy in one phase of the motion, and re lease it at another phase of the motion [39]. This property is crucial to achieving explosive motions like jumping, throwing, kicking. Thirdly, passive VIA robots can adjust the me chanical impedance of their joints to match the desired value depending on the performing task [40]. By doing so, the performance of the robot can be maximized. This is akin to impedance matching between a load and a transmission line in electrical circuits, which is done to increase the efficiency of

the electrical system. Therefore in the last 15-20 years, the researchers focused their attention on VIA actuators. Initially, the focus was mostly on the design of the VIA joints and on the investigation of their mechanical properties, while later scientists and engineers turned their attention more on the control and optimization of VIA robots. Below we briefly review the existing designs and control methods of VIA systems in the literature.

1.5 Review of Different VIA Joint Designs and Their Control Methodologies

VIA robots can be achieved by variation of either (or by a combined variation of) inertia, damping and stiffness characteristics of a joint. However, from a practical point of view, it is easier to modify the stiffness and damping of a joint, and so most of the VIA joints in the literature are based on a variation of these two parameters. Therefore, we can distinguish between *variable stiffness actuated* (VSA) joints and *variable damping actuated* (VDA) joints. VSA joints are also called variable compliance joints, where the compliance param eter is defined as the inverse of stiffness. In the literature, instead of the term variable, the words adjustable or controllable are used sometimes. Good summaries of VIA actuators are given in [33, 41]. First, we will start by reviewing the designs and control paradigms of constant stiffness actuators.

1.5.1 Series Elastic Actuators

An example of fixed stiffness actuators is the *series elastic actuators* (SEA), in which a linear spring is attached to a rigid actuator and to a link. In other words, in SEA a linear rotational and/or translational spring mechanically decouples a link from an actuator. This gives the actuator the ability to store energy and to be safe (due to lower inertia reflected on the link side), but there is no ability to adjust the stiffness and dynamics of the joint. Sometimes fixed mechanical compliance

behavior achieved by a SEA can be modified by a suitable controller design to behave as VIA. Early examples of SEA utilization include a revolute SEA from MIT [42], one degree of freedom (DOF) exoskeleton RoboKnee based on SEAs [43], non-backdrivable SEA with harmonic drive transmission [44], and Bowden cable based SEA proposed for use in exoskeleton-type rehabilitation robots [45]. Later research were focused more on control aspects [46] and improvement of SEAs [47]. For example, systematic analysis of torque control of SEAs was performed in [46], where au thors suggested to use cascaded PI controllers for the best performance. The compliant pneumatic robotic joint was realized in [48], where sliding mode control was utilized for

position control of the joint. Series and parallel elastic springs were utilized to design a powered ankle-foot prosthesis [49, 50] and a knee rehabilitation device [51]. Velocity sourced SEA, with improved performance compared to other SEAs, was presented in [52]. However, the proposed SEA consumed twice as much energy as a geared actuator. A new design of rotary SEA and its control methodology were proposed in [53, 54], where the control was achieved by employing the disturbance observer for the generation of re quired torque under time-varying conditions. Later the authors employed sliding mode control in order to overcome resistive torques and modeling uncertainties for the same ro tary SEA [55]. Simulations were performed to calculate the required joint stiffness of the soft arm, and modularized SEA was designed to match the selected joint stiffness [56].

Miniaturized rotary SEA, based on linear springs, was proposed in [57], where velocity controller would enable the SEA joint to vary its apparent impedance. Stability analysis of SEA for utilization in a haptic device was performed in [58]. Performance of SEA was compared with parallel spring configuration in [59]. It was shown that parallel spring con figuration reduces the peak power requirement of an actuator, but at the other hand increases its energy requirements. If parallel and series spring configurations are used together, then

peak power can be reduced even more, while energy requirement has value in between se ries and parallel configurations. Parallel-series elastic actuators were also used in the design of lower limb exoskeleton [60]. SEA was also used in the design of laparoscopic haptic de vice [61], of a twelve DOF Yobotics-IHMC lower body humanoid robot [62], of a hopping articulated leg [63], of a new actuator system using movable pulley for bio-mimetic sys tem [64], of micro-mechanical devices [65], of the lower body of the compliant humanoid robot “cVub” [66], and of the low-cost compliant manipulator for multi-robot systems [67] and more. Series viscoelastic actuators were used to design high-precision haptic device OSVALD in [68]. The designed haptic device offered force actuation and sensing capa bilities close to a human tactile threshold. A system of parallel SEAs, which was called distributed SEA, was proposed in [69]. It was shown that distributed SEAs require less energy, power, and torque compared to ordinary SEAs. Small and lightweight pneumatic SEA, which possesses high mechanical power output, was designed in [70, 71]. Using or thosis as an example, a paper in [72] once more proved that for human-machine interaction

compliance is necessary. A novel design of SEA, which utilizes clutch mechanism and so reduces energy consumption by 70% compared to traditional SEA, was presented in [73]. Continuously variable SEA, based on continuously variable transmission, was proposed in [74]. It was shown that continuously variable SEA is the most efficient actuator for a human knee prosthesis during ground-level walking. Variable transmission ratio based on slider-crank mechanism and SEA was utilized to design a novel prosthetic knee [75]. Advantages of SEA compared to traditional electrical motors were also shown in [76].

Force control using the model-based approach of SEA was studied in [77]. The au thors proposed a control framework, which generates necessary force/torque independent from external displacement/angle, and which has an intuitive choice of the controller pa rameters. H_∞ based control methodology for SEA was studied in [78]. Lyapunov func tions were used to control SEA in [79],

where the quadratic program was formulated as a nonlinear optimal controller, which could run at over 5 kHz. Lyapunov functions were also used in a hierarchical control scheme, whose objective was to exponentially stabilize both joint-angle and spring-torque control [80]. Closed-loop torque control of SEA was implemented in [81]. The paper contains theoretical analysis for stability and bounded ness of the proposed closed-loop control. Additionally, it includes experimental results to demonstrate the improved performance of the method compared to other existing meth ods and the increased robustness with respect to external disturbances. Finite-time torque control of SEA using the disturbance observer and continuous sliding-mode control was implemented in [82]. The Lyapunov analysis was carried out to prove the stability of the method. High performance position control of SEA, based on disturbance observer and a nonlinear sliding mode-like controller, was considered in [83]. In the proposed method, the observer was designed to estimate the modeling uncertainties and unmodeled dynamics, while the controller attenuated the estimation error and stabilized the closed-loop system. Additionally, boundedness analysis and global convergence of the proposed method were analytically proven in the paper. It was shown that model predictive controller, together with a disturbance observer, outperforms PID+disturbance observer in the SEA control problem [84]. Disturbance observer-based torque control of a Bowden cable-driven rotary SEA was developed in [85]. Model-based force control of the reaction force sensing SEA,

which was used to drive the parallel virtual ground robot, was implemented [86]. The ground robot provides virtual ground for a human standing on it, and it can interact in three directions: pitch, roll, and height. 2 DOF torque and impedance control of the cable-driven SEA was implemented in [87]. The proposed controller performed well in the presence of noise, disturbance, motor saturation, and modeling uncertainties. Open-loop and closed loop disturbance observers for SEA were compared in [88]. Motion control of a robot with integrated SEA for physical human-robot interaction applications was considered in [89].

High-performance position control of SEA using differential flatness and disturbance ob server in state-space was implemented in [90]. The authors experimentally demonstrated the high performance of the proposed controller under external disturbances such as in ertia variation, backlash, friction, and external load. Time-domain approach for control of SEA based on model reference adaptive controller and time-domain passivity approach was presented in [91]. Specifically, the authors considered stable torque control and passive impedance control of SEAs, and they demonstrated the stability of the proposed method with respect to parameter uncertainties. It was shown that disturbance observers in general lead to a better steady-state response of SEAs [92]. However, disturbance observers also lead to a degraded transient response by increasing the vibration of the end-effector. These transient vibrations were suppressed by using resonance ratio control in [92].

Guidelines for design of SEA in terms of selection of the linear spring constant are discussed in [93, 94]. New unlumped model, which uses track and pinion system, was proposed for modeling of ball screw driven linear SEA [95]. Lagrangian mechanics was utilized to derive a lumped-parameter model of SEA using the mass-spring-damper sys tem [96]. The authors showed that their model can accurately represent the SEA system under any load conditions: with low, medium or high impedance loads. Detailed internal dynamics of SEA was derived in [97], where all moving masses were modeled separately. It was shown in the paper that lumping reflected rotor inertia and the linear mass of the actuator leads to wrong assumptions about the forces at the proximal output. Next, we will briefly review the constant damping actuators.

1.5.2 Series Damping Actuators

Series damping actuator (SDA), which is an actuators with fixed damping properties, has advantages similar to SEA, such as limited impedance and safety.

However, they can not store energy, but rather absorb the energy. As a result, compared to SEA, SDA has a distinc tive advantage of impact or shock absorption capabilities, which is beneficial in some appli cations. On the other hand, this property of SDA also decreases its energy efficiency. Ad ditionally, SEA usually increases the system order by one, while SDA decreases the system order by one [98]. Therefore SDA possesses larger bandwidth than SEA. In reality, SDA can be achieved by simply connecting a damper in series or parallel to an actuator [58]. This way, the damper now decouples the link from an actuator. SDA, which was based on magnetorheological fluid, was proposed in [98]. System bandwidth and system out put impedance of magnetorheological and Newtonian viscous VDA were analyzed in [99]. Specifically, it washes shown that low bandwidth of the magneto-rheological damper to the input current compromises overall bandwidth of the system. Inverse dynamics control of magnetorheological based SDA was investigated in [100]. Authors also compared two models of magnetorheological fluids (Bingham model and Bouc-Wen model) and proposed their own modified Bingham model. The results showed that the proposed new model of magnetorheological fluid is more suitable for implementation of inverse dynamics control of SDA. Semi-active knee prosthesis with SDA was designed in [101], where SDA was used to control the swing phase of the leg and to adapt the pattern of normal human gait. Force sensing and control with high accuracy were achieved by using SDA and observer based force estimation [68]. We note that the research literature covering SDA is much less than for SEA. Next, we review the control and design of different variable stiffness actuators.

1.5.3 Variable Stiffness Actuators

Due to the aforementioned advantages of VIA robots, design of their sub-class (VSA robots) received considerable attention from the robotics community in the last 10-15 years. A common type of VSA configuration is the so-called antagonistic configuration, which is

inspired by the musculoskeletal system. In this case, two identical actuators and nonlinear elastic elements (NEEs) are necessary. These two actuators are connected to two identical nonlinear springs, which in turn are joined to a joint or link. As a result, in order to change the position of the joint, both actuators rotate in the same direction. While stiffness is var ied by changing the pretension of the springs. In other words, in antagonistic configuration, stiffness is varied by rotating the motors at opposite directions. One common disadvantage of antagonistic configuration is the high energy consumption, which is due to collinear spring force and displacement directions. One of the early examples of antagonistic VSA was designed using rolamites [102], but it was observed that physical limits of the rolamite springs constrain the joint torque and deflection. Torsion springs were utilized to design antagonistic VSA called ANLES [103], however, its stiffness variation range was rather limited 11 − 22 Nm/rad. VSA with linear stiffness behavior (quadratic force-displacement behavior) was designed using geometric shape [104]. The unique feature of this VSA is that it can be designed to have arbitrary continuous stiffness-displacement characteristics. Shape memory alloy (SMA) based VSA was proposed in [105]. SMAs have several ad vantages which make them suitable for actuator design: high force to weight ratio, high strain capability, compact and simple design. However, the stiffness variation range of SMA based VSA was rather limited: 3.1 − 3.8 N/mm. Twisted strings were utilized to design lightweight and simple antagonistic VSA [106], with the stiffness variation in the range 20 − 45 kN/m. Similar idea (with twisted strings) was used to design lightweight, high bandwidth and low torque antagonistic VSAs [107, 108].

Energy consumption of two types of VSA rotary joints was analyzed and compared in [109], where it was shown that antagonistic configuration consumes more energy than series one. VSA based on a revolute nonlinear SEA, called HypoSEA, was presented in [110]. The VSA could generate 120 Nm torque with 0.02 Nm resolution, and it could store up to 30 J of energy, but its

power-to-weight ratio was low. Mechanically adjustable stiffness actuator (MASA) based on cantilever spring was proposed in [111] for utilization in elbow rehabilitation device. Its stiffness varied in the range 50 − 250 Nm/rad, while its maximum output torque was 45 Nm. Novel VSA mechanism based on a combination of the positive and negative stiffness elements was proposed in [112]. It was shown that

a single motor can be utilized to control both the equilibrium position and stiffness of the joint in open-loop fashion. However, the mechanism cannot be implemented in systems where large output work by the motor is required. Stiffness variation of the mechanism was experimentally shown to be in the range of 20 − 130 Nm/rad. Origami-inspired soft VSA, which incorporates the pneumatic actuator and layer jamming mechanism, was pro posed in [113]. Linear springs and a transmission belt were utilized to design VSA with stiffness variation range of 400 − 2700 Nm/rad [114]. Later authors proposed the updated design of the VSA joint [115]. VSA based on Variable Torsion Stiffness was designed, and its control was performed using power analysis [116]. Specifically, the feasibility of power-optimized stiffness selection depending on task and trajectory was simulated, and position control using feedback linearization was implemented. Asymmetric antagonistic VSA, with different actuators and nonlinear elastic elements on its two sides, was designed in [117]. 1-DOF knee-actuated hopping robot was built based on the proposed VSA. Ad ditionally, energy-efficient control of the hoping robot was achieved in simulations and experiments through a PD controller with gravity compensation. Leaf springs were uti lized to design antagonistic VSA, which had the advantage that no power is required to maintain the preset stiffness [118]. The proposed VSA was controlled in velocity mode with a PI-controller. Modular, miniature, antagonistic servo-VSA (named VSA-CubeBot), with the objective of having low cost, was proposed in [119]. It could be used to design and construct multi-DOF VSA robots.

Algorithm to estimate the stiffness of antagonistic VSA robots was presented in

[120]. Currently, stiffness is mostly evaluated through mathematical models in an open-loop man ner. Energy consumption of antagonistic VSA configurations with different (linear, quadratic, exponential and cubic) springs were compared in [121]. It was shown that cubic springs require the least amount of energy, while the radius of the pulleys affect the stiffness range variation. New variable stiffness mechanism based on nonlinear deflection characteristics of buckling beams has been introduced [122]. This VSA has negative stiffness range (from −5 until 12.5 N/mm), but its deflection range is relatively low. Dielectric elastomer actu ator and low-melting-point alloy embedded silicone were utilized to design new soft VSA called VSDEA [123]. The dielectric elastomer provided bending actuation, while the al

loy was responsible for stiffness variation when heated. This VSA had a mass of 2 g, but it could lift objects with a mass of 11 g. Interesting proof of concept was demonstrated in [124], where only one actuator was utilized to control the position or stiffness of VSA called SM-VSA. This was achieved by using two small and light-weight clutches, which lock one DOF out of the two. The clutches were realized by friction belts.

In a series class of VSA joints, actuators are decoupled: one actuator controls the posi tion, while another actuator controls the stiffness. In this design class, spring force direction is parallel to the displacement needed to change the stiffness. One of the well-known ex amples of VSA in this series is the so-called MACCEPA VSA [125, 126], which could be constructed from simple components (linear spring, servomotor, gears, straight lever arm). However, stiffness of the MACCEPA had high value only at the non-deflected position, and its stiffness decreased as displacement increased. In order to solve this problem, authors proposed improved MACCEPA 2 VSA with the lever arm replaced by a profile disk, due to which MACCEPA 2 now had stiffness increasing as displacement increased [127, 128]. The stiffness variation range of the MACCEPA 2 is 0 − 170 Nm/rad. New 2-DOF modular VSA joint based on MACCEPA design, which has

two axes of rotations, was introduced in [129]. Other examples of VSA include MARIONET with independent control of com pliance and equilibrium [130]. Due to its accurate force and position control, MARIONET was later utilized to design a two-joint planar robot for home use [131]. Novel rotary-type VSA joint, called VARSC, was proposed in [132]. This VSA is actually a torque coupler, where torque transmission happens through a spring. Arched flexure and contactors were utilized to design a miniature VSA [133], which had high stiffness variation range (ratio of the highest to the lowest stiffness was 100). New VSA, which uses cam disks and rollers, was designed in the German Aerospace Center (DLR) [134]. Its stiffness variation range is 0 − 2900 Nm/rad. Similar VSA design, called QA-Joint, was implemented in [135]. Floating spring joint VSA, called FSJ VSA, is compact, lightweight and has high torque and power density capabilities [136]. It was designed in modular form with the intention to be used in the anthropomorphic DLR Hand Arm System. FSJ VSA consists of cam rollers and disks, and its stiffness varies in the range of 0 − 800 Nm/rad. New series type VSA was designed using rotary flexure shaft [137], where the variation of the second moment

of area of the shaft caused its stiffness variation. The proposed VSA did not require in put torque for holding stiffness constant and had low friction forces and inertia, while its stiffness varied in the range 280 − 1430 Nm/rad.

Another class of VSA mechanism is based on the variable lever arm mechanism. In this design, unlike as the antagonistic design and similar to series design, two actuators are decoupled: one control only position, while another controls the stiffness. The difference with the series class is that direction of displacement needed to change the stiffness is per pendicular to the spring force. Therefore, VSAs of this category are more energy efficient. In other words, with the lever arm VSA configuration, much less energy is spent on chang ing the stiffness of the system compared to antagonistic configuration. Another advantage includes the possibility to select the motors of different sizes. One of

the early examples of VSA based on lever arm mechanism includes the hybrid dual actuator unit [138, 139], with stiffness variation range of 3.9 − 120.3 Nm/rad. A new VSA, called AwAS, with the lever arm mechanism in which spring position is adjusted, was proposed in [140,141]. One motor controlled the position of the intermediate link, which sets the equilibrium position of the output link. The second motor controls the position of the linear springs, and so in effect, it controls the stiffness. Its stiffness varied in the range of 30 − 1300 Nm/rad. Similar VSA, in which spring position is a controller and which had stiffness variation in 30 − 1300 Nm/rad range, was proposed in [142]. Variable stiffness series elastic actuator with wide stiffness variation range, which also has high force-to-mass and power-to-mass ratio, was proposed in [143]. Design concept utilizing a generic port-based model for an energy-efficient VSA with the lever arm mechanism was presented in [144]. A new VSA, called CompAct-VSA, which has shorter stiffness modulation time and greater stiffness variation range was proposed in [145]. Ideally, this design has stiffness variation in the range from null until infinity, which is due utilization of the cam-based lever arm with variable pivot for adjusting the stiffness. In other words, in this design the position of the pivot point, rather than of the springs, is varied. Another VSA designs (called respectively vsaUT-II and AwAS-II) which utilize variable pivot point of the lever arm were proposed in [146–148]. These VSA designs have the advantage that stiffness modulation does not affect the energy stored in the elastic elements. Yet, another VSA design based on lever

arm mechanism with adjustable force position was proposed in [149]. The stiffness of this VSA varied in the range of 500 − 2500 N/m. A similar concept was utilized to design another VSA [150].

Recently, a new VSA based on variable lever arm mechanism with stiffness adjustment achieved through Archimedean spiral relocation mechanism was presented [151,152]. The range of stiffness variation of this mechanism is 1.7 − 150 Nm/rad. Miniaturized VSA, named mVSA-UT, based on lever arm mechanism with planetary gears was designed in [153]. A new metric, which is

helpful to compare different VSA designs in terms of energy efficiency, was introduced [154]. The metric expresses the amount of energy spent to change stiffness while the position is kept at an equilibrium configuration. Port-based power flow of different VSA designs was analyzed in [155], where a term “power-flow ratio” was introduced and it was shown that presence of pretension elements in the VSA has a negative impact on power-flow ratio. Variable lever mechanism was used to design VSA with almost linear torque-deflection characteristics at a fixed stiffness setting, while its stiffness could independently be controlled in short time [156]. Two opposite-handed torsion springs and two cam-bearing followers were used to design VSA with the variable pivot point of the lever arm mechanism [157]. The stiffness of this VSA varied from almost zero value to highly rigid. A couple of torsional springs were utilized to design compact lever arm based VSA (called pVSJ) with adjustable force position, with very wide stiffness variation range and with an infinite range of motion at the zero stiffness value [158]. A thorough review of VSA actuators and their designs is given in [33, 37, 159]. Review of DLR activities related to VSA design is summarized in [160].

VSA was utilized to design and investigate the performance of the legged hopping platform [161]. Specifically, authors investigate the relationship between stiffness, energy efficiency and stride frequency, and showed that stiffness variation is crucial in order to achieve improved behavior diversity with modest energy efficiency. Stiffness of the knee varied in the range 0.6−4.7 Nm/rad. With the advent of VSA joints, more focus was put on developing safe exoskeletons and assistive prosthetic devices. One example is the compact and modular VSA unit, based on MACCEPA VSA, which featured real-time communica tion and a new method to estimate the stiffness and torque [162]. Using this unit, 6-DOF

exoskeleton was built and experimentally tested. Pneumatic VSA based on inflatable actua tor was used to design four-stringed ukulele with audio variability [163]. Modular, cellular and stacked piezoelectric actuators were used to design VSA with tunable resonant frequen cies [164]. This VSA was shown to be durable, energy-efficient (low power consumption) and with high bandwidth. Soft

robotic gripper was built out of low-melting-point alloy, which had an order of magnitude change in its stiffness at the melting point, thus providing variable stiffness property for a gripper [165]. An interesting property of this gripper is that due to a reheating-refreezing cycle of the alloy, it can self-cure cracks and broken parts, as well as restore its mechanical properties. As a result, this gripper features self-healing properties, but its stiffness variation rate is relatively slow.

It was shown that by appropriate control of a gripper actuated by VSA, it is possible to improve the grasping ability (e.g. handle fragile and rigid-heavy objects) [166]. PID controller, which automatically tunes its proportional, integration and derivation gains de pending on the joint stiffness, was shown to have better performance in controlling VSA joints compared to PID controllers with fixed gains [167]. In this case, increased perfor mance include improved bandwidth and accuracy. Interesting work was presented in [168], where authors implemented ��∞ control of SEA to make it behave as VSA. In this way, “ap parent” stiffness of the SEA, which consists of a ball-screw cable actuator, was varied in the range from 25 − 200 Nm/rad. Control of the closed-loop (“apparent”) stiffness and damp ing of the electro-pneumatic actuator with backstepping-based algorithm was demonstrated in [169]. Using the proposed algorithm, “apparent” stiffness of the electro-pneumatic ac tuator was varied by a factor of hundred, which exceeds its real stiffness variation range. Neural network (Radial-Basis Function Network) was used to independently control the stiffness and position of the VSA joint in a closed-loop manner [170]. Bounded stability and asymptotic stability of the resulting robust adaptive controller were proven, and a slid ing mode controller was added to deal with the reconstruction error of the neural network. Simulations and experiments, which demonstrated the effectiveness of the proposed control scheme compared to classical PID control, were performed. In similar work, disturbance observer-based adaptive neural network control of VSA robot was performed [171]. Here model uncertainties were compensated for by an adaptive neural network, while nonlinear

VSA dynamics and external disturbances are compensated for by a disturbance observer. However, the experiments demonstrated that the controller suppresses the variable stiffness behavior of the joint. The state-feedback control scheme for VSA, which guarantees the prescribed performance of the tracking error, was proposed in [172]. The proposed control scheme does not need the system model, however, its feasibility was shown only in sim ulations. A new approach to control the position and stiffness of VSA robot through gain scheduling (polynomial fitting) of a set of linear quadratic regulator (LQR) gains was pro posed in [173,174]. Simulations and experiments showed that the proposed approach copes with system nonlinearities and actively damps the vibrations. A novel method to control VSA joints, which is independent of system dynamics and can take into account constraints, was proposed in [175]. However, this method is open-loop and can not guarantee achieving set objectives and adequate system performance. Open-loop stochastic optimal control of VSA joint was simulated in [176]. However, due to the lack of algorithms to numerically solve the resultant optimal control problem, the latter was solved using stochastic sampling of diffusion processes to approximate path integrals. Control strategy of VSA, which has the property that its stiffness depends on the position, with the primary goal of tracking a limit cycle trajectory was implemented in [177]. It was shown through simulations and experiments that the control law is robust with respect to external disturbances.

Virtual torque principle was used to design a PD-controller for the VSA with decoupled stiffness and position regulation [157]. Performance of passivity-based control and feed back linearization based control of torsional stiffness based VSA were compared in [178]. It was shown that feedback linearization based control is superior to passivity-based con trol in terms of accuracy and control torque. In both cases the controllers were stable, but their robustness was rather limited. Control methodology to enable a VSA (vsaUT-II) robot to catch a moving object was devised in [179]. The controller was designed to act like a damper (critically damped) in order to absorb the kinetic energy. Virtual damping coefficient and

stiffness of VSA were two control variables. However, the performance of the obtained controller was limited. VSA controller was devised to actively balance and recover in real-time a lower-body exoskeleton [180]. Balancing was achieved by an kle joint stiffness regulation and zero moment point feedback. Active vibration damping

of VSAs with weakly damped springs was demonstrated in [181], where a gain sched uled state feedback controller for the linearized dynamics along the nominal trajectory was utilized. Model-free method for damping control of VSA robots was achieved through stiffness variation [182]. The stiffness control law was derived by solving analytically the optimal control problem of minimizing the terminal energy of a single DOF spring-mass model with controlled stiffness. As a result, the bang-bang stiffness regulation mode was obtained to be optimal, which means that stiffness should be maximum when the link is slowing down and minimum when the link is accelerating. Output-feedback control of re dundant VSA robot, which requires only actuator and joint positions as a reference, was performed in [183]. End-effector workspace stiffness could be regulated by combining passive joint stiffness and active controller-based stiffness. Similar work was performed in [184], where passive stiffness in combination with active impedance control was im plemented in an optimal way in order to set Cartesian stiffness of the DLR Hand Arm System at the desired value. This method enables VSA robots to achieve a wider range of output Cartesian stiffness compared to the range obtained by pure passive VSA joint. Passive joint stiffness is controlled by a PD-controller. Control methodology to generate impulsive forces with 1-DOF manipulator using artificial fiber-type muscles and a mag netorheological brake was proposed in [185]. Authors also performed position control of the manipulator by regulating stiffness and vibration control of the manipulator by regulat ing apparent viscosity using an evaluation function. Motion planning of two-DOF planar VSA manipulator with passive noise-rejecting actuators was done in [186]. Specifically, a stochastic optimal control problem was formulated and solved by using a path integral approach, and the obtained solution was used to control the

robot in an open-loop manner. It was shown that noise can be reduced even without feedback control law. Force feedback control of pneumatic artificial muscles with guaranteed stability was performed in [187]. Additionally, authors devised mathematical formulation to compute reference force inputs for pneumatic artificial muscles for a given set of desired torque and joint stiffness inputs. In other words, with the proposed control methodology, torque and stiffness of an antago nistic joint with two pneumatic artificial muscles could be set to any desired value. A cas caded controller for an inverted pendulum bipedal robot with VSA was designed in [188],

a controller at each level controls the robot at a different level of abstraction. However, the controller could not sustain a gait for a long period of time due to foot scuffing and tripping. Finally, below we review the control and design of variable damping actuators.

1.5.4 Variable Damping Actuators

Despite the aforementioned advantages, the VSA joints have several drawbacks, which re strain their applicability. One drawback is the oscillatory motion of the output link, which is due to the absence of damping elements. This, in turn, causes the reduction of the stabil ity margin and of the control accuracy. Another drawback is the reduction of the achievable bandwidth. As a result, researchers turned their attention to damping elements, which alle viate the above problems. Similar to variable stiffness elements, variable damping elements emerged. Kevlar fiber-based VDA, called CompAct, was designed and controlled in [189], with damping variation range in $1 - 6$ Nms/rad. Kevlar fiber has the advantage of having lower stiction, higher friction coefficient, and higher wear/heat resistance. An actuator, which is capable of simultaneous and independent stiffness and damping modulation, was proposed in [190]. Authors also explored, using optimal control techniques, how variable physical damping can be exploited in the context

of rapid motions. Variable damping was achieved by electrical inductance effects in a DC motor, and the range of damping vari ation was 0 − 0.03 Nms/rad. It was shown in the paper that VDA settles to equilibrium position faster than VSA with fixed damping. VDA with fast and strong damping mecha nism and with high dissipative capacity was proposed in [191]. The proposed VDA is based on the magnitude of dry friction between aluminum and steel discs, which can be pressed against each other in a controlled manner. As a result, the damping coefficient was varied in the range of 0.01 − 0.1 Nms/rad. High viscous silicon oil, which has damping force proportional to relative speed, was utilized to design the VDA module [192], with damping variation range of 0.15 − 0.4 Nms/rad. This module was integrated with VSA-CubeBot system reported in [119]. The variable damping actuator based on hydraulic transmission with orifice effect was proposed in [193]. It was shown that the VDA can reduce the sys tem vibration while restoring the bandwidth reduced by the spring element. Novel adaptive

damping feedback control, which features two damping estimator, was presented in [194]. One damping estimator evaluates the damping of the dissipation mechanism, while the second damping estimator assesses the equivalent damping of the overall system. Precise force tracking controller for piezoelectric actuators, which possess nonlinearities such as hysteresis and creep effect, was implemented in [195]. In this paper, VDA was imple mented by using piezoelectric actuators, which generate desired frictional force, and which were controlled by simple PID-controller. Motor braking mechanism was utilized to design VDA in [196], where a variable damping torque was generated by shorting the terminals of the motor connected in parallel with VSA. By using the VSA and VDA joints, the authors designed and tested the bipedal walking robot named BLUE.

1.6 Hypothesis

From the review of control aspects of VIA robots, we concluded that VSA robots

are typi cally controlled using advanced PID, backstepping, LQR and sliding mode methods. These methods possess some drawbacks. Firstly, these control methods can not take into account system constraints and input bounds. In other words, real VIA systems possess the phys ical limitations, such as maximum input (current, voltage) and displacement/force/torque limits. Ideally, a VIA robot controller should be able to take into account the physical lim itations of the system under control. Failure to fulfill this requirement might result in the dangerous operation of VIA systems in close physical human-robot interaction settings. Secondly, due to the complexity of VIA joints, these control methods would not guarantee the utilization of VIA systems to their full extent and potential. For example, given a VSA hopping robot, these controllers would not allow us to estimate the maximum height that the robot could achieve in jumping. In other words, if a hopping robot is controlled by PID control and it achieves a certain maximum jumping height, then we would not know if this maximum height is limited due to software (controller) or it is limited by the hardware (physical limit). Thirdly, achieving the target system performance criteria is also an impor tant aspect of the control algorithms, which is not easy to accomplish with VIA systems thanks to their nonlinear, complex and constrained dynamics. As a result, in our opinion,

> the control aspect of VIA systems is mostly unsolved. If this problem is left unresolved, then VIA systems might still pose a danger for a human, which means that VIA systems will not provide a full solution to a problem for which they were designed in the first place. Additionally, solving these control problems would accelerate the start of the fourth in dustrial revolution (Industry 4.0), which envisions widespread and common close physical human-robot interaction taking place in the future. Even though the benefits of solving these problems would be the most vivid in the humanoid robotics community, their effect might trickle down almost to all branches of robotics community and other engineering fields, including chemical, process and aerospace engineering. The main hypothesis of the thesis is to utilize optimization tools to solve control problems of VIA robots.

Specifically, we will tackle the control aspect of VIA systems using optimal control problem formula tion coupled with model predictive control algorithms. Hypothetically, the proposed con trol methodology (framework) would solve most of the abovementioned control problems related to VIA systems. In other words, optimization algorithms would enable utilization of VIA systems to their full extent, satisfy the system constraints, be general (applicable to any VIA system) and ensure that the set performance is satisfied. This research might lead to the following possible future impacts: widespread utilization of VIA robots, fast growth of physical human-interaction-oriented soft robots, acceleration of start of Industry 4.0.

Due to rapid progress in deep learning, reinforcement learning, and big data, alter native research directions, like reinforcement-based control, data-driven control, machine learning-based control, have recently gained attention in control and robotics communi ties [197–202]. These control methods should also be tried and tested for control of variable impedance actuated robots. However, this is outside the scope of this thesis.

1.7 Thesis Organization

The thesis is organized as follows. In the next Chapter 2, we will describe the dynamics of VSA robots and their closed-loop control framework based on nonlinear model predic tive control (NMPC). Specifically, the chapter begins by presenting the procedure to model the dynamics of VSA robots, then it is followed by the formulation of the optimal control

problem (OCP) for any task. The OCP is solved off-line, and the obtained solution corre sponds to the optimized system performance subject to the objective function and system constraints. This is followed by the detailed presentation of the model predictive control framework, whose aim is to ensure that the system follows the reference trajectory obtained by the OCP. The description of the case

study, where we present the modeling of the pla nar two-link VSA robot manipulator, is followed next. This part also contains information about simulations and experiments that we performed in order to test the proposed con trol framework. After that, simulation and experimental results are presented. Chapter 3 describes the NMPC applied to the reaction-wheel augmented VSA. The chapter starts by reviewing the literature on the application of braking torques to alter the dynamics of robots and other systems. Then modeling of VSA robots augmented with the reaction wheels is derived and presented, which is followed by the description of the single-link planar VSA robot manipulator augmented with the reaction wheel, which is used as a test-bed. Sim ulations and experiments were performed in order to test the feasibility of our proposed control method, the results of which are presented at the end of the chapter. Chapter 4 covers the formulation and solution of the time-optimal control problem for VSA systems. Firstly, two time-optimal control problems are formulated: minimum-time for target per formance and minimum-time for maximum performance. After, methods to solve these two OCPs are discussed, which is followed by the description of two experimental setups utilized to test these control methods. The chapter concludes by presenting the simulation and experimental results. Energy-optimal control problem of VSA robots is considered in Chapter 5. The chapter beings by the formulation of three energy-optimal control problems: maximum performance with limited energy, target performance with minimum energy, and maximum performance with minimum energy. Then the experimental system is described, which is followed by a presentation of simulation and experimental results. Linearized model predictive control is given in Chapter 6, which describes a procedure to linearize and discretize nonlinear system, followed by a derivation of quadratic programming prob lem. Experiments and the corresponding results are described at the end of the chapter. Finally, the thesis is concluded in Chapter 7, which briefly summarizes the main contri bution of the current work and presents a description of how the outcome of the research

might influence the robotics community. 45

Chapter 2

Closed-Loop Control of Variable Stiffness Actuated Robots via Nonlinear Model Predictive Control

2.1 Introduction

Despite recent technological advances, robots are still outperformed by humans in tasks re quiring dexterity, safety, and efficiency. Robots could be utilized in areas such as medical, search and rescue, and social robotics due to human-like performance. This would also allow industrial robotics to shift to a new paradigm, in which humans and robots are work ing side by side collaboratively and safely without the requirement of protective barriers. Anthropomorphic robots were designed by researchers inspired by the potential to achieve human-level performance [203]. Initially, researchers focused on studying the kinematic configuration of the robots. Later the research focused on their dynamic and transient behavior in situations such as collisions, physical interaction with humans, objects and the environment. One approach is the design of robots with low inertia, with integrated force/torque sensors and active torque control [204]. These robots have inherent limita tions [160], in spite of the presence of successful and already commercialized examples. Firstly, the links are not mechanically decoupled from the actuators in the joints, and com

pliant behavior is achieved by active control. Therefore, the torque limits of the

gearbox and actuators might be exceeded during short-lasting impacts, and presumably, the system might be damaged. Secondly, unlike the human musculoskeletal system, these robots do not have the capability to store energy induced in their link-side structure. Therefore their velocity and dynamic force are limited in tasks such as throwing, jumping and running.

VSA robots [102, 114, 134, 136, 205–207] have emerged recently in order to cope with the challenges faced by the actively torque-controlled light-weight robots. VSA robots are usually intrinsically compliant, and energy is stored by elastic elements in the joints. Therefore, the compliant robots can reduce energy consumption in repetitive tasks, increase maximum generated force and velocity capabilities, and absorb impacts easily. Moreover, the robot joints and the human can be protected by the variable stiffness behavior of the robot. However, these advantages are also accompanied by certain shortcomings: the de sign becomes more complicated due to the need for incorporating elastic elements and the respective additional actuators. Additionally, higher elasticity leads to a reduction of the mechanical bandwidth and of the absolute position accuracy. The task planning, parameter identification, and control of VSA robots are also challenging problems. Due to coupled nonlinear dynamics, a high number of control inputs and actuation constraints, intuitive tuning of the controllers cannot guarantee utilization of the full potential of VSA robots. The latter can be achieved by exploiting the natural dynamics of the system, for which the controller optimally modulates the stiffness of the joints/actuators during operation. For example, controllers based on this idea were used to improve human-robot interaction safety, increase performance in explosive movement tasks and decrease energy consump tion [174, 208–210]. A general framework for the optimal control of compliant robots was introduced in [1]. In that work, firstly, the motors with fast dynamics were controlled in closed-loop. Then, the closed-loop motor dynamics with actuation constraints were incor porated into the complete dynamic description of the VSA robot. Later, with the aim of carrying out a specific task, a sequence of reference actuator positions was determined by solving an optimal control problem ([211]) offline.

Full closed-loop control would be needed to deal with the presence of external distur bances and imprecise information of the model parameters (hereafter, both of them together

would be simply referred to as *uncertainties*) [1]. A closed-loop control law for VSA robots should be able to handle multivariable coupled nonlinear systems, and simultaneously tak ing all the constraints into account, while updating the control law at each sampling time based on measurements of sensors. The best candidate with the aforementioned character istics is model predictive control (MPC) [212]. Nonlinear MPC (NMPC) is needed due to the intrinsic nonlinear dynamics of VSA robots. However, NMPC has the drawback of re quiring (at each sampling time) the solution of a non-convex optimization problem. Faster and more reliable solvers are available for convex optimization problems, which can instead be formulated in case of linear MPC. For a general overview on a convex and non-convex optimization problem, a reader is referred to [213]. Solving a numerical optimization prob lem is typically a computationally expensive task. Therefore, linear and nonlinear MPC have been traditionally utilized to control slow processes, such as in chemical plants, with sampling intervals in the order of seconds or minutes (see, e.g., the survey [214]). Control ling robotic systems, on the other hand, typically requires much shorter sampling intervals. The difficulties associated with the combined presence of computational complexity and short sampling interval perhaps constitute the main reason why NMPC, to the best of our knowledge, has never been experimentally implemented for VSA robots.

The described situation is changing rapidly due to recent progress in efficient solvers and formulations for fast MPC, and due to the availability of more powerful microproces sors. The use of MPC (especially for the simpler case of linear systems) is now being expanded from the classical process control applications to areas requiring faster sampling rates such as mechatronics, automotive, and power electronics [215–221].

This chapter is based on our paper by Zhakatayev et al. [222]. Our main contribution in this chapter is the development and experimental verification of an NMPC-based frame work for controlling VSA robots. As a first step, an optimal control problem (OCP) is generated after obtaining a dynamical model of the robot similarly to [1]. This is done in order to obtain the sequence of input and state values that minimize the cost function associated with the considered task. However, instead of directly providing the control sequence into the system in an open-loop fashion, the time evolution of the robot links generated via OCP (referred to as *ideal trajectory* in the following) is used as a reference to

be tracked by an NMPC controller. The overall block scheme of the proposed control law (the details of which will be explained in the remainder of the chapter) is shown in Fig. 2- 1. For comparison, Fig. 2-1 also depicts the partially open-loop approach proposed in [1]. Based on real-time data from the sensors, the NMPC controller generates the closed-loop control inputs by running an a-priori fixed number of iterations of a finite-horizon optimal control problem (FHOCP) at each sampling instant. The implementation of a fixed number of iterations of the numerical solver, leading to inexact or sub-optimal solutions, is usually sufficient to obtain a satisfying performance. This is also supported by theoretical results on the closed-loop stability using inexact numerical solutions [223–225].

We specifically refer to the ACADO tool [226, 227] in order to provide a general ap proach for running NMPC in a framework that can be easily utilized for different VSA robots. This choice is dictated by different reasons: ACADO is open source, provides a rather intuitive syntax in C++, implements high-performance numerical solvers, and al lows the designer to generate the controller routine in C++.

As a case study, the control of a two-link VSA manipulator actuated by four motors via four nonlinear elastic elements is considered. Given a fixed time interval available for the robot motion, the goal is to maximize the distance at which a ball attached to the end effector is thrown. Simulations and real-world

experiments, in which external disturbances or parameter variations are present, are conducted to evaluate the effectiveness of our ap proach compared to the scheme proposed in [1].

The chapter is organized as follows: Sec. 2.2 briefly recalls the main concepts related to the modeling of VSA robots. Section 2.3 contains the description of OCP, while the MPC problem is formulated and discussed in Section 2.4. Case study is presented in Section 2.5 and the chapter is concluded in Section 2.6.

2.2 Modeling of VSA Robotic Systems

Two sets of coordinates have to be considered in order to model the VSA robots. Like in standard rigid manipulators, a first set $\theta \in R^{n}$ represents the joint angles of the robot. Another set of coordinates $\varphi \in R^{n}$ accounts for the motor angles of the compliant actu

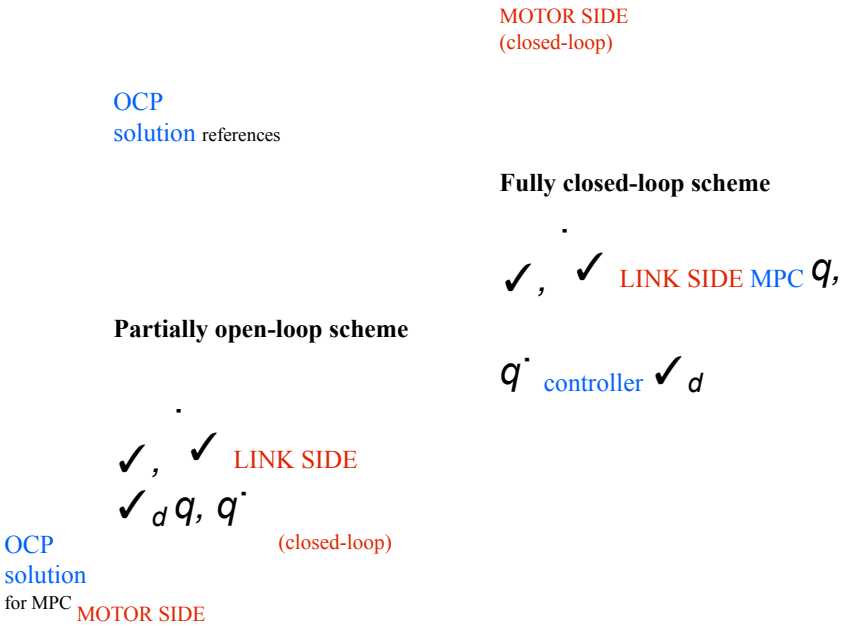

Figure 2-1: Comparison between the partially open-loop scheme of [1] and the proposed NMPC-based fully closed-loop scheme.

ators, taking into account also the gear reduction. Vectors θ and q are referred to as the *link-side* and *motor-side* coordinates, respectively [1]. Using the Lagrangian formalism, the link-side dynamics is described by

$$B(q)\ddot{q} + C(q, \dot{q})\dot{q} + F\dot{q} + g(q) = \tau_{sa}(q, \theta) \quad (2.1)$$

where $B(q) \in \mathbb{R}^{n \times n}$ is the inertia matrix of the rigid part of the robot ($B = B^T > 0$), $C(q, \dot{q}) \in \mathbb{R}^{n \times n}$ describes the contribution of normal inertial forces and Coriolis forces, $F\dot{q} \in \mathbb{R}^n$ accounts for the viscous friction, while $g(q) \in \mathbb{R}^n$ contains gravity force terms, and $\tau_{sa}(q, \theta) \in \mathbb{R}^n$ is the vector of the joint torques generated by the elastic elements that affect the link-side dynamics. The motor-side dynamics is typically faster than the link-side dynamics, and since the stiffness modulation depends on the value of q, a separate control loop is usually employed for the position control of the motor side. The torque generated by each motor becomes a function of the motor variables θ and $\dot{\theta}$, and of the reference angular positions, namely $\tau_m \in \mathbb{R}^n$. This torque constitutes the "physical" input to the system. It is well known that the closed-loop dynamics of each motor can be represented by a linear second-order model under the standard assumption of high gear reduction, and/or of high gain feedback position controllers, as

$$\ddot{\theta}_i + 2\zeta_i \omega_i \dot{\theta}_i + \omega_i^2 \theta_i = \omega_i^2 q_{i,d}, \quad i = 1, \ldots, n \quad (2.2)$$

where θ_i and $q_{i,d}$ are the i-th components of θ and q_d, respectively, while $\zeta_i, \omega_i \in \mathbb{R}_{>0}$ are constants associated with each motor dynamics. The values of these constants can be related to the parameters of the actuators and of their position controllers (see, e.g. [1, Sec. III]). Typically,

position control is already implemented in the available commercial servomotors. In order to obtain the fastest possible response with no overshoot, these servomotors often are tuned such that the closed-loop dynamics is critically-damped, i.e., $\zeta = \zeta$.

We define the state vector

$$[\ \theta,\ \dot{\theta}\ \ddot{\theta}\ ] \in R^{n_q},$$

and the input vector τ , $\tau_{max} \in R^{n_q}$in order to obtain an overall nonlinear state-space model of the system. Let K , $diag\{2\tau_{max}\} \in R^{n_q \times n_q}$ and D , $diag\{\tau^2_{max}\} \in R^{n_q \times n_q}$. Finally, the state-space model of the system is

$$\dot{x} = f(x, u) = \begin{bmatrix} \dot{\theta} \\ -M^{-1}(\theta)(C(\theta, \dot{\theta})\dot{\theta} + g(\theta) - K\tau + D\theta) \end{bmatrix} \quad (2.3)$$

where $C(\cdot, \cdot)$ is a continuously differentiable function with respect to its both arguments.

2.3 OCP for VSA Robotic Systems

It is natural to define tasks formulated as OCPs for the control of VSA robots. The goal of the OCP is to find the optimal realization $\tau^*_{open}(t)$ of the desired open-loop input sequence $\tau_{open}(t) \in R^{n_q}$ within a fixed time interval

[0, $\tilde{t}$), $\tilde{t}$ ∈ $R_{>0}$. In our case, $u_{ref}(t)$ is assumed to be a piecewise-constant valued signal with fixed discretization step t_s ∈ $R_{>0}$. More specifically, given k ∈ $Z_{\geq 0}$,

$$u_{ref}(t) = u_{ref}(t_k), \ \forall \ t \in [t_k, (k+1)t_s). \quad (2.4)$$

We assume that $\tilde{t}$ is an integer multiple of t_s, i.e., there is $\tilde{k}$ ∈ $Z_{>0}$ such that $\tilde{t}$ = $\tilde{k}t_s$. As a result, all information contained in $u_{ref}(t)$ for t ∈ [0, $\tilde{t}$) can be summarized by the finite sequence

$$u_{ol}, \{u_{ref}(0), u_{ref}(t_s), \ldots, u_{ref}((\tilde{k}-1)t_s)\}. \quad (2.5)$$

u^*_{ol} denotes the corresponding optimal sequence. Then the OCP can be written as

$$u^*_{ol} = \arg\min_{x(0),u_{ol}} J(x(\cdot), u_{ol}) \quad (2.6a)$$

$$\text{subject to } x(t) = x(0) + \int_0^t f(x(\tau), u_{ref}(\tau))d\tau \quad (2.6b)$$

$$x(t) \in X, \ \forall t \in [0, \tilde{t}] \quad (2.6c)$$

$$u_{ref}(t) \in U, \ \forall t \in [0, \tilde{t}). \quad (2.6d)$$

here, the cost function is usually defined as

$$J(x(\cdot), u_{ol}) = h(x(\tilde{t})) + \int_0^{\tilde{t}} l(x(t), u_{ref}(t))dt. \quad (2.6e)$$

The term $h(\cdot)$, also called *Mayer term*, is related to the terminal state. Mayer term can be used, for example, to impose the minimization of the distance error at time $\tilde{t}$ of the end effector with respect to a reference position. On the other hand,

$\Phi(\cdot, \cdot)$, also called *Lagrange term*, accounts for the behavior of the robot during the whole task. Lagrange term can be used, for instance, in order to minimize energy consumption, or the actuators wear. In general, the sets $\tilde{\mathcal{X}}$ and $\tilde{\mathcal{U}}$ are defined in order to take into account limits on an gular positions and velocities of the motors and links, displacement of the elastic elements, input currents and etc. For VSA robots it is of paramount importance to guarantee sat isfying these constraints. A control strategy, which does not guarantee fulfillment of the constraints, can easily lead to temporary/permanent damage of the robot and/or of the ex ternal object. The optimal open-loop input signal $u^{*}_{ol}(t)$ for $t \in [0, \tilde{T})$, together with the corresponding evolution of the state variables $x_{ol}(t)$, are obtained from the sequence u^{*}_{ol}.

OCP is solved numerically by discretizing continuous evolution of the state with a given number of sub-intervals. Later, numerical integration algorithms, such as Runge

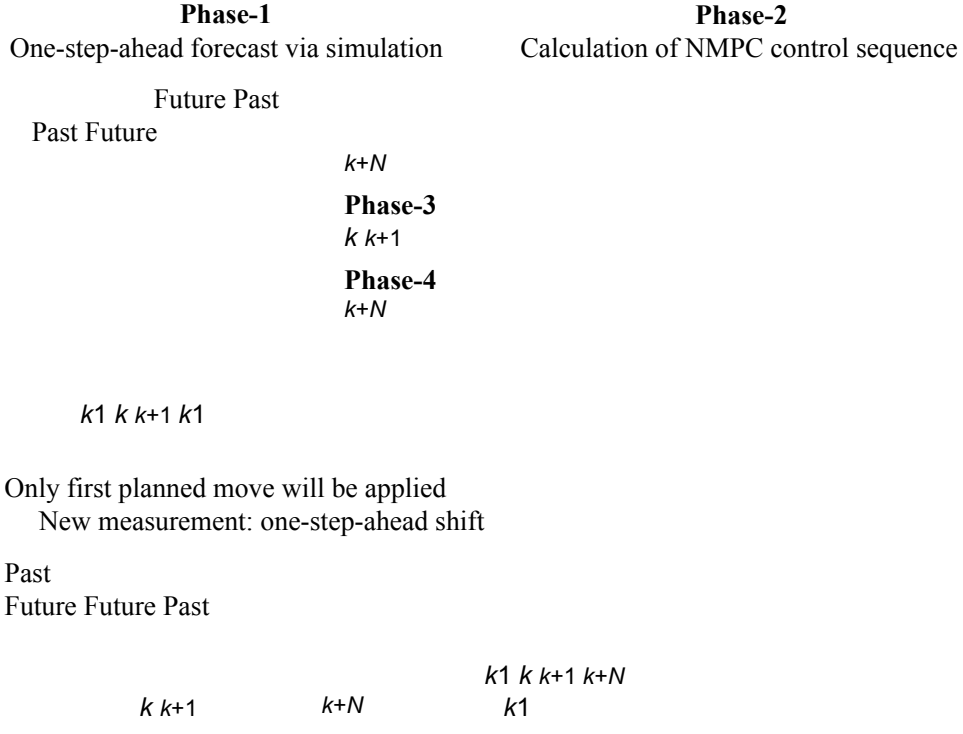

Figure 2-2: Different phases of the NMPC control law computation for closed-loop control. Detailed expla nations of the phases are presented in Section 2.4.1.

Kutta methods [228] implemented in ACADO Toolkit, are employed. OCP solution is obtained by solving a nonlinear optimization problem, for which different approaches ex ist [211]. In this chapter the so-called *multiple shooting* approach is utilized. Multiple shooting approach exploits the structure of the discretized nonlinear optimization problem and condensing techniques [229]. We limit our concise description of the numerical solvers to those implemented in ACADO [226], even though their different versions could be em ployed. Numerical solvers implemented in ACADO use sequential quadratic programming (SQP) based on quasi-Newton Hessian approximations. The tool qpOASES is used to solve the underlying quadratic programs [230].

2.4 Closed-Loop Control Framework

2.4.1 NMPC Formulation

As already mentioned, the direct application of ��(��) to the system can lead to results which are different from those expected, due to the presence of external disturbances and model mismatches. The solution proposed here consists of introducing a closed-loop controller for the overall robot dynamics. NMPC controller uses the evolution of the variables of interest obtained by solving the OCP (ideal trajectory) as reference. After recording the measured values of all the state variables, the controller runs a finite number of iterations of a FHOCP at each of the fixed time instants $\text{}\text{} = \text{}\text{}\text{}\text{}\text{}_{\text{}\text{}}$. Here $\text{}\text{}_{\text{}\text{}}$ is the sampling interval, which coincides with the discretization step of the OCP, while $\text{}\text{} \in Z_{\geq 0}$. As in the case of the OCP control input, the generated control

variable ◻◻(◻◻) is assumed to be a piecewise-constant signal, i.e.,

$$◻◻(◻◻) = ◻◻(◻◻◻◻_{◻◻}),\ \forall\ ◻◻ \in [◻◻◻◻_{◻◻}, (◻◻ + 1)◻◻_{◻◻}). \quad (2.7)$$

A conceptual diagram of how the NMPC control law functions is shown in Fig. 2-2, in which a single state and control variable are present and all time indices are normalized by $◻◻_{◻◻}$ for clarity. Each phase is explained in detail in the following.

One-Step Ahead Forecast via Simulation

Let us denote the time intervals needed to obtain the state value from the sensors as $◻◻_{◻◻◻◻◻◻◻◻◻}$, to determine the value of the next control move as $◻◻_{◻◻◻◻◻◻◻◻◻}$, and to transmit the computed input command to the actuators as $◻◻_{◻◻◻◻◻◻◻◻◻}$. For robotics applications, these three time intervals are not necessarily negligible with respect to the sampling interval of $◻◻_{◻◻}$. Therefore, to assume that ◻◻(◻◻◻◻$_{◻◻}$) can be computed based on the measurement of ◻◻(◻◻◻◻$_{◻◻}$) and instantaneously applied to the system at time ◻◻◻◻$_{◻◻}$ is not correct and feasible. Instead, we propose the control law, which is computed using the state value at time (◻◻ − 1)$◻◻_{◻◻}$ and is applied to the system at time ◻◻◻◻$_{◻◻}$ under the reasonable assumption that

$$◻◻_{◻◻◻◻◻◻◻◻◻} + ◻◻_{◻◻◻◻◻◻◻◻◻} + ◻◻_{◻◻◻◻◻◻◻◻◻} \leq ◻◻_{◻◻}. \quad (2.8)$$

The system performance would degrade if the control law, obtained with a delay of $◻◻_{◻◻}$, is directly applied without taking into account the evolution of the system states during the sampling time. Instead, the proposed solution is shown in Fig. 2-2 (Phase 1). The ideal state trajectory (from OCP) to be tracked is depicted as the solid green line. The grey band on the left represents the past. The measured past values of the state variable are shown as red dots, while the past control moves applied to the system are represented as the piecewise-constant red signal. When time enters the yellow band, which represents the current sampling interval, a control input (black constant signal

within the yellow band) is applied, which had been computed during the previous sampling interval by NMPC. At $tt = 0$, since there is no NMPC move computed before, one can apply $uu(tt) = uu_{seq}(tt)$ for $tt \in [0, \Delta tt_{ss})$, in the fair assumption that $uu(0) \approx uu_{seq}(0)$. In general, at the beginning of each sampling interval, a measurement of the current state variable $xx((kk-1)\Delta tt_{ss})$ is acquired (shown as a black dot in Fig. 2-2 (Phase 1)). Instead of initiating computing the NMPC law that will be applied at time $kk\Delta tt_{ss}$ from the measured state value, the control routine simulates the system dynamics for one sampling interval, which usually requires a computationally negligible effort. This single sampling time simulation is represented as a purple line in Fig. 2-2 (Phase 1), which terminated at the blue dot representing the estimate of $xx(kk\Delta tt_{ss})$, computed as

$$\hat{xx}(kk\Delta tt_{ss}) = xx((kk-1)\Delta tt_{ss}) + \int_{(kk-1)\Delta tt_{ss}}^{kk\Delta tt_{ss}} ff(xx(tt), uu((kk-1)\Delta tt_{ss}))\,dtt. \quad (2.9)$$

This is a very basic strategy to effectively handle time delays in NMPC (for a discussion of the topic, the reader is referred to the introduction of [231]).

Calculation of NMPC Control Sequence

The main purpose of the FHOCP is to determine an optimal realization of $uu(tt)$, namely $uu^{*}(tt)$, in the interval $tt \in [kk\Delta tt_{ss}, (kk + NN)\Delta tt_{ss})$, based on $\hat{xx}(kk\Delta tt_{ss})$ as initial condition. Here $NN \in Z_{>0}$ ($NN \ll \tilde{NN}$) is called *prediction horizon*. The whole information contained in $uu(tt)$

for $tt \in [kk\Delta tt_{ss}, (kk + NN)\Delta tt_{ss})$ can be summarized by the finite sequence

$$u(\text{□}_{\text{□}}) \triangleq \{\text{□}(\text{□}_{\text{□}}), \text{□}((\text{□}+1)\text{□}_{\text{□}}), \ldots, \text{□}((\text{□}+\text{□})\text{□}_{\text{□}})\}. \quad (2.10)$$

due to the piecewise-constant nature of the control law. Using a standard notation, the cor responding input control sequence $u^*(\text{□}_{\text{□}})$ is found by running a finite number of iterations of the FHOCP defined in the following

$$\underset{\hat{\text{□}}(\text{□}_{\text{□}}),u(\text{□}_{\text{□}})}{\text{minimize}} \Phi(\text{□}(\cdot), u(\text{□}_{\text{□}})) \quad (2.11a)$$

$$\text{subject to } \text{□}(\text{□}) = \int_{\text{□}}^{\hat{\text{□}}(\text{□}+\text{□})} \text{□}(\text{□}(\text{□}), \text{□}(\text{□}), \text{□}(\text{□}), \

$$+\int_{(\mathrm{tf}+\mathrm{tp})\mathrm{fpp}}^{\mathrm{fpp}}\left(\left\|\mathrm{qm}(\mathrm{tp})-\mathrm{qm}_{\mathrm{d}}(\mathrm{tp})\right\|_{\mathrm{Qm}}^{2}+\left\|\mathrm{q}(\mathrm{tp})-\mathrm{q}_{\mathrm{d}}(\mathrm{tp})\right\|_{\mathrm{Q}}^{2}\right)\mathrm{dtp} \quad (2.12)$$

where $\mathrm{Qm} \in \mathrm{R}^{\mathrm{nm}\times\mathrm{nm}}$, $\mathrm{Q} \in \mathrm{R}^{\mathrm{n}\times\mathrm{n}}$, $\mathrm{R} \in \mathrm{R}^{\mathrm{nu}\times\mathrm{nu}}$ are selected such that Qm, $\mathrm{Q} \geq 0$, and $\mathrm{R} > 0$. The desired evolution of the system variables is represented by the functions $\mathrm{qm}_{\mathrm{d}}(\mathrm{tp})$ and $\mathrm{q}_{\mathrm{d}}(\mathrm{tp})$, defined for $\mathrm{tp} \in [0, \mathrm{tf}]$. One possibility could be to completely draw them from the OCP solution, i.e. $\mathrm{qm}_{\mathrm{d}}(\mathrm{tp}) \equiv \mathrm{qm}_{\mathrm{fpp}}(\mathrm{tp})$, and $\mathrm{q}_{\mathrm{d}}(\mathrm{tp}) \equiv \mathrm{q}_{\mathrm{fpp}}(\mathrm{tp})$. As an alternative, we propose the

following approach:

- The state variables of the link-side dynamics (i.e., q and $\dot{\mathrm{q}}$) are typically related to the task performance. Therefore, their evolution obtained by the OCP should be tracked as closely as possible. As a result, the values of the first $2\mathrm{nq}_{\mathrm{d}}$ components of q_{d}, which describe the reference values for q and $\dot{\mathrm{q}}$, should coincide with the first $2\mathrm{nq}_{\mathrm{d}}$ components of $\mathrm{q}_{\mathrm{fpp}}(\mathrm{tp})$.

- The state variables related to the motor-side dynamics (i.e., qm and $\dot{\mathrm{qm}}$) are usually “in termediate variables” between the control input signals and the link-side state vari ables. For this reason, the values of the last $2\mathrm{nq}_{\mathrm{d}}$ components of q_{d}, which describe the reference values for qm and $\dot{\mathrm{qm}}$, can be set as constant signals, corresponding to the values leading to the minimum wear of the robot elements. For example, the refer ence position for an actuator can be the one for which a nonlinear spring connected to it is uncompressed, while its reference velocity can be set to zero. Ideally, these values are not actual references as in the case of the link-side variables:

instead, the controller should simply operate as close as possible to these values, as far as the tracking of the link-side variables is correctly performed.

· The reference control variables $\mathbf{q}_{d}$ (reference angular and/or linear positions given to the servomotors) can also be set as those which cause the minimum wear, force/torques in the system and/or energy consumption of the system.

Finally, the weight matrices $\mathbf{Q}$, $\mathbf{R}$, and $\mathbf{P}$ in (2.12) will be described. Usually, they are cho sen as diagonal matrices, and we also follow this approach. For example, $\mathbf{Q}$, diag$\{\bar{q}_{1}, \ldots, \bar{q}_{2n}\}$ implies

$$\|\mathbf{x}_{d}(\mathbf{k}) - \mathbf{x}_{d}(\mathbf{k})\|^{2}_{\mathbf{Q}} = \sum_{i=1}^{2n} \bar{q}_{i} \left(x_{di}(k) - x_{di,d}(k)\right)^{2}$$

meaning that the weight of every state variable is determined by the element of the corre sponding diagonal matrix. $\bar{q}_{i}$ denotes the elements of the diagonal matrix $\mathbf{Q}$, and those of $\mathbf{R}$ are referred to as $\bar{r}_{i}$. The main purpose of the NMPC controller is to track as closely as possible the ideal evolution of the link-side state variables. Therefore, in order to obtain small tracking errors, $\bar{q}_{i}$ for $i = 1, \ldots, 2n_{d}$ should be chosen with much larger magnitude

than $\bar{q}_{i}$ for $i = 2n_{d} + 1, \ldots, n$. The same values of $\bar{q}_{i}$, $i = 2n_{d} + 1, \ldots, 2n_{d} + n_{d}$ (i.e., those relative to $\mathbf{q}$) can be utilized in $\bar{q}_{i}$, $i = 1, \ldots, n_{d}$. Larger values of $\bar{q}_{i}$ would reduce the tracking error during the prediction horizon, whereas larger values of $\bar{q}_{i}$ would lead to the greater importance of the tracking error at the end of the prediction horizon. One can impose $\mathbf{P} = \mathbf{Q}_{d}\mathbf{Q}$ in order to weight the tracking error at $(k + N)n_{d}$ as the tracking error in one of the sampling intervals of the prediction horizon, but different formulations can be chosen depending on the specific task.

Only the First Planned Move Will Be Applied

The whole determined sequence u(□□□□$_{□□}$) is not utilized directly: instead, following the so called *receding horizon* principle, only the first control move is applied to the system. This first control move is calculated for □□ ∈ [□□□□$_{□□}$,(□□+1)□□$_{□□}$), namely □□$^{*}_{□□□□}$(□□□□$_{□□}$) (Fig. 2-2 (Phase 3)).

New measurement: one-step-ahead shift

When the new sensor measurement is acquired, the control input just computed by NMPC is applied, and the horizon window used for the prediction of the system is shifted one sampling interval ahead (this can be seen by the time indices in Fig. 2-2 (Phase-4)). A new one-step ahead simulation is run, together with a new FHOCP. The term *receding horizon* describes what is realized in steps 3 and 4, and is derived from the one-step-ahead shift of the prediction window. This is a key and an important concept, that makes MPC a fully closed-loop technique. MPC is also referred to as “receding horizon control” for this rea son. The measured state represented as the black dot in Fig. 2-2 (Phase-4), in general, has a different value than the corresponding state value expected from the one-step simu lation. This means that, due to the presence of unmodeled uncertainties and disturbances, the actual evolution of the system dynamics is slightly different than the expected.

The method employed to solve the FHOCP is similar in principle to the one used for solving the OCP. For instance, the evolution of the state dynamics is discretized, and the resulting nonlinear optimization problem is run with a fixed number of iterations by mul tiple shooting using SQP. SQP, in turn, runs a fixed number of iterations of the underlying

quadratic program with qpOASES. However, the difference is that while in the OCP case the optimization algorithm could take, in principle, as long as required, in a closed-loop NMPC implementation for robotic systems, only a few

milliseconds would be typically available. By utilizing the warm-starting of the FHOCP (i.e., using the information on the solution obtained at the previous sampling time to initialize the optimization problem at the current time) and by using relatively small values of horizon window ��, in the available computation time, an acceptable solution can be obtained. If due to problems in reading the sensors or computational issues, a solution of the FHOCP is not provided within the sampling interval, the second NMPC input computed at the previous sampling time can be applied to the system. This comprises an intrinsic fault tolerance property of the control scheme, which can run for a few consecutive iterations in an open loop manner. We re fer an interested reader to [231–233] for further details on the real-time iteration scheme implemented in ACADO software.

2.4.2 Remarks on Theoretical Guarantees

We follow a standard practice in MPC applications in order to use a simple and non conservative NMPC formulation. That is, we apply a strategy that does not give any theo retical guarantees on recursive feasibility and closed-loop stability in the presence of uncer tainties, and we experimentally test its effectiveness as it will be shown in the case study. Nonetheless, in the following we prove a basic result, which in the ideal case guarantees perfect tracking.

Proposition 1 *We assume that the solution of the OCP* (2.6)*, namely* ��$_{����}$(��) *and* ��$_{����}$(��) *for* ��$\in$ [0, ~��]*, has been obtained for system* (2.3)*. By solving the FHOCP* (2.11) *online for* ��$=0,\ldots,$ ~�� $-$ ��*, an NMPC controller is then utilized to track the link-side dynamics. Assume, for the sake of simplicity, that* ��$_{��}$(��) $\equiv$ ��$_{����}$(��)*,* ��$_{��}$(��) $\equiv$ ��$_{����}$(��)*, and that the number of iterations that FHOCP performs is large enough so that at each sampling time its optimal solution is achieved. Also,* ��$\supseteq$ ~�� *and* ��$\supseteq$ ~��*. If* ��(0) = ~��(0)*, and* ��(��) *is generated by solving the FHOCP* (2.11)*, then* ��(��) $\equiv$ ~��(��)*, for all* ��$\in$ [0, ~��].

Proof: The input $\hat{u}(t) \equiv u^*_{opt}(t)$ is applied to the system during the time interval $t \in [0, T_s)$. 60

Since we assume that the system dynamics is exactly represented by (2.3), one has $\hat{x}(t) \equiv x^*_{opt}(t)$ for $t \in [0, T_s]$. Being $\hat{x}(T_s) = x^*_{opt}(T_s)$ and $N \geq \tilde{N}$, $n \geq \tilde{n}$, then $x^*_{opt}(T_s) = \tilde{x}^*_{opt}(T_s)$ is a feasible solution of (2.11) for $N = 1$. Moreover, setting $x^*_{opt}(T_s) = \tilde{x}^*_{opt}(T_s)$ leads to $\Phi(\tilde{x}(\cdot), u^*(0)) = 0$, which means that $\tilde{x}^*_{opt}(T_s)$ is the global minimizer for the FHOCP that will be ideally determined by the optimization algorithm. The perfect tracking of the state variables in $t = [T_s, 2T_s]$ is achieved by the application of this solution, and, in particular, it yields $\hat{x}(2T_s) = \tilde{x}(2T_s)$. The same reasoning can be applied in sequence to all subsequent steps. Therefore, the proposition is proved by induction.

We expect a nearly perfect tracking of the link-side variables in the nominal case if only the link-side components of the state are taken as references from the OCP solution, and the weight terms $\bar{q}_s$ and $\bar{r}_s$ associated with them are much larger than the other weight terms. In this case, the evolution of the motor-side variables and of the input signals can follow a different pattern as compared to the OCP solution. Also, in the perturbed case, we expect that the tracking performance will slowly degrade as the importance of the uncertainties increases. However, we also expect better performance in the perturbed case than applying the OCP control sequence in an open-loop fashion.

2.5 Case Study

2.5.1 System Modeling

A two-link planar manipulator, actuated by four servomotors and with a ball attached to the end effector (Fig. 2-3), is considered as a test robot in our case

study. Four servomotors are connected to an equal number of nonlinear elastic elements (NEEs). Firstly, we analyze the link-side dynamics (2.1), and the vector of link-side angles is defined as $\theta = [\theta_1 \ \theta_2]' \in R^2$. The inertia matrix $M(\theta)$ can be written as

$$M(\theta) = \begin{bmatrix} M_{11} & M_{12} \\ M_{12} & M_{22} \end{bmatrix} \quad (2.13)$$

with

$$M_{11} = I_1 + m_1 r_{c1}^2 + I_2 + m_2(r_1^2 + 2 r_1 r_{c2} \cos\theta_2 + r_{c2}^2) + m_3(r_1^2 + 2 r_1 r_2 \cos\theta_2 + r_2^2)$$

$$M_{12} = I_2 + m_2(r_{c2}^2 + r_1 r_{c2} \cos\theta_2) + m_3(r_2^2 + r_1 r_2 \cos\theta_2)$$

$$M_{22} = I_2 + m_2 r_{c2}^2 + m_3 r_2^2$$

where I_{ci}, m_{ci}, r_{ci}, l_i are, correspondingly (for link $i = 1, 2$), its moment of inertia around the center of mass, its mass, its length, and the length from the center of mass of the link up to its joint center, while m_3 is the ball mass. Also,

$$C(\theta, \dot{\theta}) = \begin{bmatrix} m_3 r_2) r_1 \sin\theta_2 \, \dot{\theta}_2 & -\dot{\theta}_1 - \dot{\theta}_2 \\ -(m_2 r_1 r_{c2} + & 0 \end{bmatrix}, \quad (2.14)$$

and

$$B = \begin{bmatrix} b_1 & 0 \\ 0 & b_2 \end{bmatrix}, \quad (2.15)$$

where b_1 and b_2 denote viscous damping constants. Finally,

$$K(\theta) = \begin{bmatrix} k_1 & k_2 \\ \end{bmatrix}, \quad (2.16)$$

where τ_1 , $\tau(\tau_1 \tau_{c1} + \tau_2 \tau_1 + \tau_3 \tau_1) \cos \tau_1 + \tau(\tau_2 \tau_{c2} + \tau_3 \tau_2) \cos(\tau_1 + \tau_2)$, and τ_2 , $\tau(\tau_2 \tau_{c2} + \tau_3 \tau_2) \cos(\tau_1 + \tau_2)$.

Variable-stiffness behavior of each of the two joints is achieved by antagonistic config uration of the NEEs. As a result, each joint has two NEEs (Fig. 2-4). The vector of elastic joint torques τ_τ is

$$\tau_\tau = \begin{bmatrix} \tau_1 \tau_2 \\ (\tau_1 - \tau_2) \\ (\tau_4 - \tau_3) \end{bmatrix} = \tau \quad (2.17)$$

where τ_τ, τ = 1, .., 4 is the tension in each of the four tendons, and τ is the joint (pulley) radius, which is the same for both joints. NEE 1 and NEE 2 are attached to the first joint,

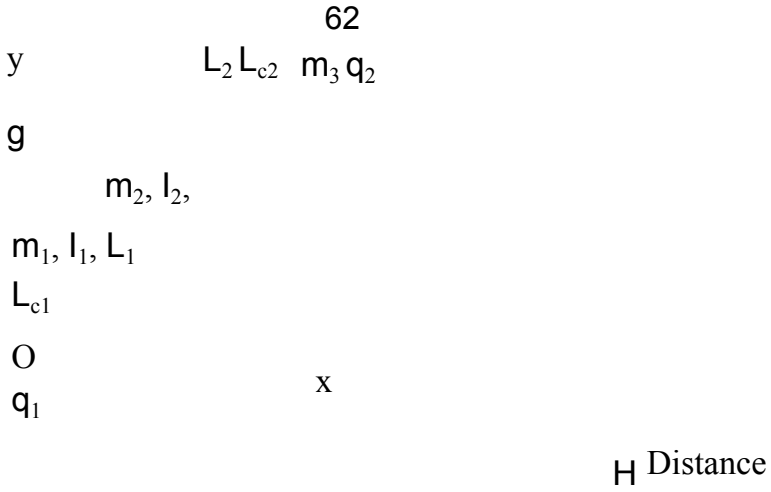

Figure 2-3: Schematic drawing of the two-link planar manipulator.

Figure 2-4: Schematic drawing of an antagonistic joint, connected to two motors via nonlinear elastic ele ments (NEEs). Parameters outside and inside of parentheses are for joint 1 and joint 2, respectively.

while NEE 3 and NEE 4 are attached to the second joint, see Fig. 2-4. Each NEE is designed and constructed such that the tendon tension is quadratic polynomial function of the tendon displacement: $\square\square_{\square\square} = \square\square_{\square\square}\square\square_{\square\square}^{2} + \square\square_{\square\square}\square\square_{\square\square} + \square\square_{\square\square}$, $\square\square = 1, .., 4$, where $\square\square_{\square\square}$, $\square\square_{\square\square}$, $\square\square_{\square\square}$ are coefficients (NEE parameters) and $\square\square_{\square\square}$ is the tendon displacement. The values of $\square\square_{\square\square}$ can be estimated from joint geometry and system parameters as $\square\square_1 = \square\square_0 - \square\square(\square\square_1 + \frac{\square\square}{\square\square}_2) + \square\square_{\square\square}\square\square_1$, $\square\square_2 = \square\square_0 + \square\square(\square\square_1 + \frac{\square\square}{\square\square}_2) - \square\square_{\square\square}\square\square_2$, $\square\square_3 = \square\square_0 + \square\square\square\square_2 + \square\square_{\square\square}\square\square_3$, $\square\square_4 = \square\square_0 - \square\square\square\square_2 - \square\square_{\square\square}\square\square_4$, where $\square\square_0$ and $\square\square_{\square\square}$ are, respectively, initial displacement of NEEs and the radius of pulleys on motors (which is the same for all motors). Variable compliance actuation is ensured by antagonistic configuration and nonlinear behavior of the NEEs. Overall, the system in form (2.3) has twelve state variables and four input variables.

2.5.2 Experimental Setup

The robot described in the previous Section was built as a prototype (shown in Fig. 2-5) in order to conduct real-world experiments to show the performance of our scheme. Solid works software was used to design the robot. Links and joints were machined from textolite (a type of composite epoxy material) and steel, correspondingly. Motor and joint pulleys, and motor holders were printed using Objet Connex 260 3D printer. Four Dynamixel MX 28T motors with 67 revolutions per minute no-load speed and 2.4 Nm stall torque were used as actuators. USB2Dynamixel module connected to the USB port of the control com puter was used for communication between the motors and the control computer. Joint and motor angular positions were measured by six AMT-102V capacitive incremental encoders with a resolution of 1024 pulses per revolution. Three National Instruments (NI) PCI-6221 cards acquired the encoder measurements. BK Precision 1761 DC Power supplies were used to provide 12 V to the motors and the electromagnet and 5 V to the encoders. A sim ple circuit containing a power transistor was built to drive the electromagnet for holding and releasing the ball, and it was controlled via a digital output of one of the PCI-6221 cards. The experimental setup was assembled on an aluminum breadboard (Thorlabs PBH51506). The connections between the joint pulleys and the NEEs, and between the NEEs and the motors were made using polyethylene fibers (Spectra) rated for a load of 400 N. A tennis

ball, with a steel plate attached to it, is used as the ball at the end of the electromagnet.

All the manufactured components of the robot were weighed using electronic weight scale before the assembly in order to determine the parameters of the system. Dimensions, volume, moment of inertia and center of mass of different parts of the robot were deter mined using SolidWorks. The friction coefficients

($\mathbf{\Omega}_1$ and $\mathbf{\Omega}_2$) of the joints were determined experimentally by recording the joint angles during free oscillations of the links and then finding best fit damping coefficient. Additional experiments were performed to characterize each NEE. Specifically, in these experiments Dynamixel MX-28T motor was pulling each NEE by fixed small step-size increments, while a force gauge sensor (Extech Instruments 475055) was utilized to record force measurements at each step. The recorded experimen tal force-displacement measurements were used to fit a quadratic curve, the parameters of which were utilized later in OCP and MPC formulations.

Accordingly, the values of the link-side system parameters were found to be: $\mathbf{\Omega}_1 = 0.330$ m, $\mathbf{\Omega}_2 = 0.433$ m, $\mathbf{\Omega}_{\mathbf{\Omega}1} = 0.116$ m, $\mathbf{\Omega}_{\mathbf{\Omega}2} = 0.222$ m, $\mathbf{\Omega}_1 = 0.674$ kg, $\mathbf{\Omega}_2 = 0.307$ kg, $\mathbf{\Omega}_3 = 0.074$ kg, $\mathbf{\Omega}_1 = 5.08 \cdot 10^{-3}$ kg·m^2, $\mathbf{\Omega}_2 = 6.92 \cdot 10^{-3}$ kg·m^2, $\mathbf{\Omega}_1 = 0.0124$ N·m·s, $\mathbf{\Omega}_2 = 0.0064$ N·m·s, $\mathbf{\Omega}_1 = 12400$ N/m^2, $\mathbf{\Omega}_1 = 1360$ N/m, $\mathbf{\Omega}_2 = 13600$ N/m^2, $\mathbf{\Omega}_2 = 1350$ N/m, $\mathbf{\Omega}_3 = 5320$ N/m^2, $\mathbf{\Omega}_3 = 1500$ N/m, $\mathbf{\Omega}_4 = 13700$ N/m^2, $\mathbf{\Omega}_4 = 1410$ N/m, $\mathbf{\Omega}_{\mathbf{\Omega}} = 0$, $\mathbf{\Omega} = 1, .., 4$, $\mathbf{\Omega} = 0.013$ m, $\mathbf{\Omega}_{\mathbf{\Omega}} = 0.026$ m, $\mathbf{\Omega}_{\mathbf{\Omega}\mathbf{\Omega}\mathbf{\Omega}\mathbf{\Omega}\mathbf{\Omega}\mathbf{\Omega}} = 0.025$ m, $\mathbf{\Omega}_0 = 0.005$ m. As for the motor side dynamics, the parameters in (2.2) for the Dynamixel MX-28T motors were determined by system identification to be $\mathbf{\Omega}_{\mathbf{\Omega}} = \mathbf{\Omega}_{\mathbf{\Omega}} = 40.0$.

2.5.3 OCP Formulation

The main objective of the OCP is to maximize the distance $\mathbf{\Omega}$ at which the ball is thrown, given a fixed time interval $\mathbf{\Omega}\tilde{}$ = 4 s for the motion (which, with the given sampling time $\mathbf{\Omega}_{\mathbf{\Omega}} = 20$ ms, leads to $\mathbf{\Omega}\tilde{}$ = 200). The value of $\mathbf{\Omega}$ at any time instant during the robot motion
can be found as

$$\mathbf{\Omega} = \mathbf{\Omega}_{\mathbf{\Omega}} + \dot{\mathbf{\Omega}}_{\mathbf{\Omega}}\dot{\mathbf{\Omega}}_{\mathbf{\Omega}} + \sqrt{\dot{\mathbf{\Omega}}_{\mathbf{\Omega}}^2 + 2\mathbf{\Omega}(\mathbf{\Omega}_{\mathbf{\Omega}} + \mathbf{\Omega})}\ \mathbf{\Omega}, \quad (2.18)$$

Figure 2-5: Experimental setup of the two link planar robot with variable stiffness actuators. D1 and D2 show the attachment points of the disturbance magnets to links 1 and 2, respectively. P indicates the extra mass connection points for parameter variation experiments.

where $h_0 = 0.813$ m is the height from the ground to the frame origin, $g = 9.81$ m/s^2, and

$$x_{ee} = l_1 \cos(q_1) + l_2 \cos(q_1 + q_2)$$

$$y_{ee} = l_1 \sin(q_1) + l_2 \sin(q_1 + q_2)$$

$$\dot{x}_{ee} = -l_1 \sin(q_1)\, \dot{q}_1 - l_2 \sin(q_1 + q_2)(\dot{q}_1 + \dot{q}_2)$$

$$\dot{y}_{ee} = l_1 \cos(q_1)\, \dot{q}_1 + l_2 \cos(q_1 + q_2)(\dot{q}_1 + \dot{q}_2).$$

We would like to limit the energy consumption during the robot motion while trying to maximize $v(\tilde{x})$. The energy consumption of a motor increases as each motor velocity $\dot{q}_j$ and torque $\tau_j = \tau_{sj} \tau_{lj}$ increases, since the elastic potential energy of each NEE is $E_j = \int \tau_{sj} \, d\tau_{sj}$. Therefore, quadratic terms relative to motor velocities and torques are also considered in

the OCP cost function (2.6e), as follows

$$J(x(\cdot), u_{ol}) = \int_0^{\tilde{t}} \left(\sum_{j=1}^{4} \left(\alpha_j \dot{q}_j^2 + \beta_j \tau_{sj}^2 \right) - v(\tilde{x}) \right) dt \quad (2.19)$$

where, in order to suppress high-frequency oscillations of the links, we set $\alpha_j = \beta_j = 5 \cdot 10^{-2}$. Higher values for these parameters would lead to more conservative solutions, while lower values would lead to energetic and impulsive behavior. The sets $\tilde{X}$ in (2.6c) and $\tilde{U}$ in (2.6d) are expressed in the following, where we directly refer to the physical quantities. State constraints are written as,

$$\tilde{\mathcal{X}} = \left\{ \begin{array}{l} \mathbf{x} \in \mathbb{R}^{12} : \\ -170\pi/180 \le q_1 \le -10\pi/180 \text{ [rad]} \\ -90\pi/180 \le q_2 \le 90\pi/180 \text{ [rad]} \\ -5 \le \dot{q}_m \le 5 \text{ [rad/s]} \\ 0.005 \le q_m \le 0.025 \text{ [m]} \\ 0 \le \tau_m \le 1.4 \text{ [Nm]} \end{array} \right\}$$

where $i = 1, \ldots, 4$. The inequalities are imposed to prevent exceeding physical joint mo tion limits, to limit motor velocities and torques (the imposed values are compatible with the Dynamixel MX-28T motor, and verified experimentally), and to limit spring compres sion. Notice that all these inequalities can be directly expressed as only depending on the state vector. The set of input constraints

$$\tilde{\mathcal{U}} = \{ \mathbf{u} \in \mathbb{R}^4 : 0 \le u_{i,k} \le 2\tau \text{ [}\ldots\text{]}, i = 1, \ldots, 4 \}$$

is imposed to avoid multiple motor rotations, which in turn prevents tendon tear. Vertical hanging position of the two links ($q_1 = -\pi/2$, $q_2 = 0$), zero link and motor velocities, initial motor and reference motor positions corresponding to initial NEE displacements were used as the initial condition $\mathbf{x}(0)$ for the OCP. We used the ACADO toolkit (Version 1.2.0) with the solver options described in Section 2.3 for our task. The KKT tolerance (used for the termination criterion of the SQP algorithm) was set to 10^{-5}. The computation time of the OCP was approximately 22 minutes on a desktop computer with 2.4 GHz Intel Xeon E5620

processor and 16 GB of memory.

2.5.4 MPC Formulation

It is mentioned in Section 2.4.1 that the primary objective of the NMPC controller is to track the OCP evolution of the link-side variables. In order to formulate the NMPC law, we set a prediction horizon $N = 10$, which implies a prediction time of 200 ms with 20 ms sampling time. Definition of the cost function (2.12) requires the desired evolution of state and control variables, which has been defined as follows. Since the evolution of the link side variables is strictly related to the throwing task, the components of q_{ref} relative to q and $\dot{q}$ for the two links are used as reference for the corresponding variables of the MPC problem. As for the other state variables, the reference values for $\dot{q}$ were set to zero, while the references for q_m and τ were set to values corresponding to minimum spring compression, in order to limit energy consumption and wear of the springs. The weight matrices have been defined as $Q = \mathrm{diag}\{1, 1, 0.1, 0.1, 10^{-6}, 10^{-6}, 10^{-6}, 10^{-6}, 10^{-4}, 10^{-4}, 10^{-4}, 10^{-4}\}$, $R = \mathrm{diag}\{10^{-6}, 10^{-6}, 10^{-6}, 10^{-6}\}$, and $Q_N = P Q P^T$.

Evolution of input and state variables determined by OCP is often close to the boundaries of sets $\tilde{U}$ and $\tilde{X}$. These bounds can be violated in practice due to the presence of uncertainties. Therefore, some of the boundaries used for the OCP solution were expanded in the MPC formulation, in order to give additional flexibility to the MPC controller to be able to compensate the effect of uncertainties, as mentioned in Section 2.4.1:

$$
\begin{aligned}
&-210\pi/180 \le q_1 \le 30\pi/180 \text{ [rad]},\\
&-120\pi/180 \le q_2 \le 120\pi/180 \text{ [rad]},\\
&0 \le \dot{q}_m \le 5, \text{ [rad/s]}, \quad 0.025, \text{ [m]}.\\
&1.6 \text{ [Nm]}, \quad 0.003 \le\\
&-5 \le \dot{\tau}_m \tau_m \le
\end{aligned}
$$

$$
x \in \mathbb{R}^{12}:
$$

Using these settings, the MPC controller is generated through ACADO Toolkit in

the form of C++ code and Matlab/Simulink block variants. In both cases, the MPC controller is synthesized according to Section 2.4.1, and the fixed number of iterations of the FHOCP

solver in each sampling interval is set to 10.

2.5.5 Simulation Results

We test both schemes of Fig. 2-1 in the Simulink environment in order to compare the framework proposed in [1] with our proposed approach. For the open-loop case, the input signals obtained from the OCP solution are fed to a Simulink model of the plant. For the closed-loop case, the MPC controller is implemented by a specific Simulink block generated by ACADO. MPC controller interacts with the Simulink block, which models the planar VSA manipulator. For both cases, the piecewise-constant control signals are defined with T_s = 20 ms, while the ODE4 (Runge-Kutta) solver of Simulink is employed with fixed-step size set of 0.2 ms.

As a first example, both schemes are applied to the system, which is simulated using exactly the same state equations (2.3) employed in the OCP and in the MPC controller. These results are not presented, but in this nominal case, the open-loop scheme perfectly tracks the link-side references, while the closed-loop scheme generates a negligible error. These results are expected, because perfect tracking even in the nominal case would be obtained only if $q_m(t) \equiv q_{link}(t)$ and $\dot{q}_m(t) \equiv \dot{q}_{link}(t)$. However, in our implementation, the reference q_m for the motor-side variables in the MPC controller does not coincide with the OCP solution. This also causes the reference positions $q_{m,i}$, i = 1, .., 4 to be different than in the OCP, but it occurs because a different solution is obtained, which nonetheless leads to a similar evolution of the link-side variables. We obtained the thrown distance of d = 3.80 m for the open-loop scheme, while for the closed-loop scheme d = 3.77 m is obtained (due to less than perfect tracking).

As a second example, the effect of additive external disturbance terms is considered. Specifically, two disturbance torques ⬚1(⬚) and ⬚2(⬚), of constant but different magnitude, are applied to joints 1 and 2, respectively, simultaneously in the interval ⬚ = [0.2, 0.6] s. In order to get a map of ⬚ as a function of disturbance magnitudes and directions, the ampli tude of the disturbance torques were varied for different simulation instances. Each external torque magnitude is independently varied from −0.5 N·m to 0.5 N·m in 21 intermediate

Figure 2-6: Distance thrown as a function of external disturbances applied at two joints (a,b) and of added parameter variation (c,d).

values. The magnitudes of these disturbances is in the same range as the joint torques gen erated by the actuation system, and can represent for example the interaction of the robot with an external object during the task execution. The upper row of Fig. 2-6 shows the results of ⬚ versus disturbance torque simulations. In the open-loop case, (Fig. 2-6a), the thrown distance is in general lower than the nominal value of 3.80 m, despite the fact that, ⬚ slightly exceeds that of the nominal case for a few disturbance combinations. Moreover, the link positions exceeded the imposed constraints in some simulations, which in real life might cause damage to the system. The closed-loop system achieves the nominal ⬚ for most combinations of disturbances, as shown in Fig. 2-6b. This is especially evident for com binations of disturbances with similar direction and with values close to maximum ±0.5 N·m torque, where for the closed-loop system ⬚ is 3.80 m, while for the open-loop system it is close to 1.50 m. The performance of the closed-loop system is slightly worse than the performance of the open-loop system only for disturbance combinations with opposite sign

and with magnitude close to 0.5 N·m.

As a third example, a parameter variation was taken into account. The masses of the first link (⬚1) and of the second link (⬚2) were varied in a

range of ±25% with respect to their nominal value with 21 intermediate values in order to obtain ﷺ as a function of pa rameters. For the open-loop case, Fig. 2-6c, the results show that the distance values lower than the ideal ﷺ were obtained for most of the parameter variation combinations. However, ﷺ achieves the ideal value or even exceeds it slightly for some values of parameters (ﷺ_1 is large while ﷺ_2 is close to nominal). This might be explained as increasing ﷺ_1 leads to higher inertia of the first link, and thus to higher kinetic energy at the last swing before ball release, which in turn increases ﷺ. For the closed-loop system using the MPC controller, Fig. 2-6d shows that in most conditions the nominal distance is achieved, except for param eter values when ﷺ_1 is at the lower and ﷺ_2 is at the higher end of the range, for which ﷺ decreases to 3 m. Similar to the second example, it was observed that for some parameter combinations, the open-loop control caused constraint violation, whereas this was not the case for the closed-loop control.

As expected, compared to the open-loop scheme, the proposed scheme manages to limit performance degradation. The difference between the nominal distance from OCP and the distance obtained in the simulation was computed for each point of the graphs in Fig. 2-6. The root mean squares of this difference are 0.62 m, 0.29 m, 0.66 m, 0.16 m for the results shown in Figs. 2-6a, 2-6b, 2-6c, and 2-6d, correspondingly.

2.5.6 Experimental Results

For real-world experiments, open-loop and closed-loop implementations of the robot task were written in C++. The control task is run with a sampling time of 20 ms in both pro grams. The control task is enforced using high-resolution native timer routines of Mi crosoft Windows (QueryPerformanceCounter API). For the open-loop system, the input signals obtained from the OCP solution are sent directly over the USB2Dynamixel module to the motors at every time step. For the closed-loop experiments, firstly motor and link encoders are read at each sampling time. Secondly, the robot model is simulated for one

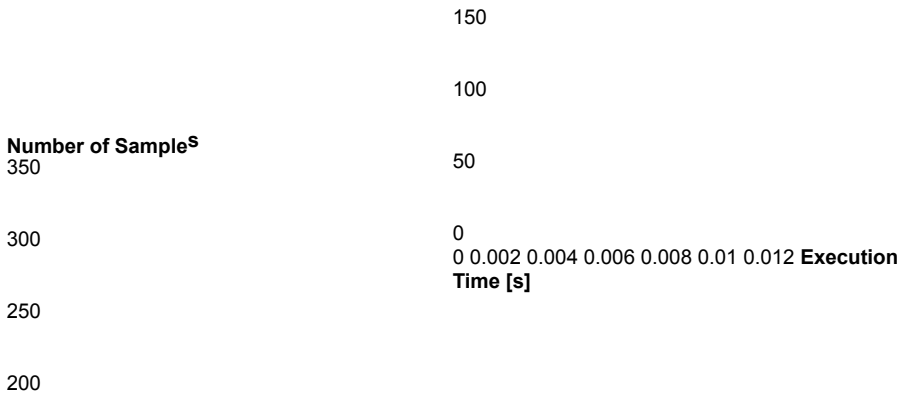

Figure 2-7: Histogram of execution times needed to run the NMPC control routine in the real world exper iment. Notice that the maximum execution time is significantly smaller than the sampling interval Δt_s = 20 ms, which constitutes the upper bound.

sampling time to compute the one-step-ahead forecast (Section 2.4.1). Thirdly, using the ACADO generated code block, the NMPC control sequence is computed (Section 2.4.1). Fourthly, the first move of this sequence (Section 2.4.1) is applied to the system by sending the motor commands via the USB2Dynamixel module. In both open-loop and closed-loop experiments, the electromagnet is turned off to release the ball at $\tilde{t}$ = 4 s. If the con dition in (2.8) is satisfied, the system can maintain the 20 ms control loop. In order to check this condition during closed-loop experiments, t_{s1}, t_{s2} and t_{s3} were recorded at each sampling time of six experimental trials resulting in 1200 instances of these three time intervals. The total execution time of the closed-loop controller at each sampling time is equal to their sum (i.e. $t_{s1} + t_{s2} + t_{s3}$). A histogram generated using these data is shown in Fig. 2-7. The results show that the maximum execution time is less than 20 ms, which satisfies (2.8), and that our approach is real-time feasible for the specific task.

Open-loop and closed-loop controllers were experimentally tested for three scenarios: nominal case (i.e., without uncertainties except those intrinsically present in the modeling inaccuracies), with external disturbances and with added

parameter variation. Compared to the 3.80 m of the ideal ball thrown distance, in the nominal case, distances for the open-loop and closed-loop control were 2.05 m and 3.22 m, correspondingly. Fig. 2-8

depicts reference, open-loop and closed-loop control joint positions and velocities, and the corresponding motor positions, for the nominal case. It can be observed that, compared to the open-loop variant, the closed-loop controller closer tracks the joint positions and velocities, which are the link-side parameters enforced by the controller and also directly effecting the task performance. On the other hand, the deviations of the motor positions from their corresponding references (not directly affecting the task performance) are larger in the closed-loop case than in the open-loop case. This is explained by the fact that the NMPC controller tries to achieve better link-side tracking under uncertainties. The superior performance of the closed-loop system can be attributed to its inherent robustness to these uncertainties.

Both links were disturbed independently in the first 1.5 s of the experiments aim ing to assess the performance of both schemes in the presence of external disturbances. Neodymium magnets were used to generate the disturbances. One magnet was rigidly at tached to each link (resulting in two magnets for two links). Other two similar magnets were rigidly installed inside two separate plastic structures (one magnet for each plastic piece). The plastic structure was connected to the rigid part of the experimental setup using a tendon similar to the ones used for motor connections. The timing of the disturbances was tuned by the slack on these tendons. The supplemental material video shows the appli cation of the disturbances using the magnets. The force at which the plastic structures with magnets detach from the link was measured between 1.2 N and 1.6 N. The resulting max imum disturbance torques applied to the joints have values near 0.5 Nm. The mass of the cubic neodymium magnet with a 5 mm edge dimension is around 1 g. Therefore, weights of the magnets can be considered negligible compared to the weights of the links. Due to the

disturbance, the performance of both schemes degrades obviously. Specifically, in the open-loop experiment the thrown distance was 1.63 m (0.42 m less than the corresponding real-world experiment in the nominal case), while for closed-loop this distance was 3.04 m (0.18 m less than the real-world experiment in the nominal case), which is almost double value of the open-loop case. The reference, open-loop and closed-loop control joint posi tions and velocities, along with the corresponding motor positions for the disturbance case, are shown in Figure 2-9. It can be observed that after the disturbance is applied, the devi

ation of the open-loop controlled system from the reference link-side trajectories is higher than the closed-loop one. From the motor positions, it can be observed that the closed-loop controller acts to compensate against the disturbance. The advantage of NMPC control for disturbance rejection over the open-loop control is clearly demonstrated by this example.

Finally, the performance of both schemes was determined by testing them in the pres ence of parameter variation. By attaching four M8 screws with nuts to the specially de signed slots (see Fig. 2-5), the weight of the second link was increased. Each screw and nut couple weighs around 18 g, which results in 72 g weight increase of the second link (this is approximately equivalent to 23% increase of the original link weight). The resulting distance for the open-loop experiment with parameter variation was ⬚ = 1.57 m, while for the closed-loop experiment ⬚ = 2.71 m was obtained. Compared to the nominal case, link and motor side trajectories for the open-loop scheme display increased deviations from their corresponding optimal reference trajectories (Fig. 2-10). Link and motor positions still closely follow the reference trajectories for the closed-loop experiment. Compared to the nominal case, the decrease of the thrown distance due to added parameter uncertainty is more than the one due to external disturbances. This can be explained by the fact that the external disturbances act only for a finite (usually brief) period of time, and, given enough time to compensate for it, the MPC controller is able to steer the system back to the nom inal trajectory. On the other hand, the added parameter variation is similar to the

effect of disturbances that act all the time when the robot motion is happening. As a result, it is more difficult to compensate for the effect of parameter variations.

The thrown distances for the considered scenarios are summarized in Table 2.1. One can notice that the ideal thrown distance (obtained from simulation) is not reached in ex periments, even though the closed-loop MPC scheme achieves larger distances than the partially open-loop approach. We speculate that this might be due to oversimplification of the system model (e.g., the intrinsic dynamics of the NEEs, such as friction and hystere sis, are not considered), and/or due to errors in obtaining the parameters of the model (it is difficult to precisely measure the damping coefficient). These issues might be allevi ated, to some extent, by adaptive control schemes for on-line parameter estimation and/or developing system identification methods geared for VSA robots.

A video containing the real-world experiments can be found in [234], which also qual itatively conveys the performance of our approach.

Table 2.1: Open-loop and closed-loop thrown distance ﬀ (m) for the ideal case (from simulation), and the three real-world experiments (nominal, external disturbance and parameter variation).

	Ideal	Nominal	Disturbance	Parameter
Open loop	3.80	2.05	1.63	1.57
Closed loop	3.77	3.22	3.04	2.71

2.6 Conclusions

A framework for the closed-loop control of VSA robots based on NMPC has been intro duced and analyzed. It has been shown, using simulations and real-world experiments, that the proposed scheme presents a lower sensitivity to uncertainties with respect to the state of-the-art approach [1]. Basic theoretical results have been proved in the nominal case, and to demonstrate the practical applicability of the presented work, a case study including simulations and real-world experiments has been presented. In the next chapter, we will describe

the dynamics of VSA robots with the reaction wheels and their closed-loop control framework based on nonlinear model predictive control.

75

Figure 2-8: Reference, open-loop and closed-loop joint positions and velocities, and motor positions in the nominal case.

76

Figure 2-9: Reference, open-loop and closed-loop joint positions and velocities, and motor positions when external torque disturbances are applied at the joints from 0.2 s to 0.6 s.

77

Figure 2-10: Reference, open-loop and closed-loop joint positions and velocities, and motor positions when extra mass is added to the second link as parameter uncertainty.

Chapter 3

Augmenting Variable Stiffness Actuation Using Reaction Wheels

3.1 Introduction

A higher degree of autonomy for robots is envisioned by the smart manufacturing paradigm Industry 4.0. Rather than executing preprogrammed tasks rapidly and repetitively, robots will work with humans in close proximity and also learn from them to execute new tasks and optimize their performance [235, 236]. The recent surge of interest in physical human robot interaction research is motivated by this expectation. In order to address the safety concerns during this interaction, soft robotics emerged as a branch of robotics [237]. Active compliance is one way of achieving soft robot behavior. In active compliance control, the manipulators regulate joint behavior under closed-loop control using data from torque and force sensors [204]. However, a variety of factors, such as the controller sampling time, sensor response time, noise, and robot link inertia, cause limitations of active safety [160]. Additionally, active compliance control does not make a rigid robot manipulator intrinsi cally safe, and if a controller fails, then undesirable consequences might happen. Building upon the series elastic actuator concept of

the 90's [42], variable stiffness actuated robots were introduced to overcome the limitations of actively torque controlled robots [114]. An inherent characteristic of VSA robot design is its passive yet dynamically adjustable com pliance. Decoupling of links from actuators via nonlinear elastic elements is the recurring

design philosophy of numerous VSA robot implementations [37]. VSA robots possess the following advantages over rigid actively torque controlled counterparts:

1. *Safety* needs to be explicitly embedded into the control systems of the traditional po sition controlled and also actively torque controlled rigid robots during their physical interaction with humans. VSA robots come with intrinsic safety, thanks to their me chanical design, which physically separates the actuators from the links [34]. If we assume that limits on the link velocities are enforced through design and/or control, then human-friendly operation of VSA robots can be ensured by setting low joint stiffness [238]. Additionally, due to the presence of the elastic elements in VSA joints, they gain shock absorption capability. Shock absorption reduces the prop agation of impact forces during collisions with stiff objects to the fragile parts of the actuator and drive-train assembly. This way, the damage to the robot and the environment is also bounded.

2. *Dynamic adaptation* of joint compliance gives the ability to VSA robots to optimize their performance for specific tasks. Gait dynamics in robotic locomotion was tuned by mechanically adjustable joint compliance to achieve energy efficiency and robust ness [125, 239]. The importance of compliance adjustment of human fingertips for dexterous manipulation was discussed in [240]. For explosive tasks, optimal stiffness modulation was essential to achieve high link velocities [241].

3. *Energy efficiency* is achieved by the energy storage capability of the compliant ele ments present in VSA robots [144]. Kinetic energy

accumulates in the elastic ele ments as potential energy, which can be released later when necessary. Novel VSA mechanisms for energy-efficient hopping, a cyclical task, at a wide spectrum of stride frequencies were presented in [242] and [243].

Mechanical design of VSA robots, as well as their control, are challenging and also are non-trivial. Traditional control approaches are ineffective with respect to VSA robots due to high nonlinearity of the elastic joint-link coupling and the presence of input and state constraints. Recently, progress was made in the control of VSA robots by defining and